UNIVERSIDAD VERACRUZANA

FACULTAD DE FÍSICA

Wehrl Entropy around avoided crossings in the Lipkin-Meshkov-Glick model

Trabajo recepcional en la modalidad de:

TESIS

que como requisito pacial para obtener el título de:

Licenciado en Física

P R E S E N T A

ISAIAS SILICEO GUZMÁN

ASESORES:

Dr. Daniel Julián Nader
Dr. Sergio Adrián Lerma Hernández

Xalapa Enríquez, Veracruz Enero 2023

To my mother Lety

Acknowledgements

Elaborating this thesis project would not have been possible without the constant support of Dr. Daniel Julián Nader and Dr. Sergio Adrián Lerma Hernández, who from the first day for a year have shared with me their knowledge in physics and programming. I sincerely appreciate your patience, time and advice, as well as the trust you have placed in me by allowing me to be part of this research project in this area of Physics. Furthermore, i want to thank Dr. Meenu Kumari for help and feedback during the calculations and results, also for reviewing this project. Finally, i want to thank M. in Physics Humberto Vázquez Sánchez for reviewing this project and remarks.

To my family and friends:

Estudiar física ha sido el proyecto más grande de mi vida hasta ahora y no habría sido posible sin el apoyo incondicional de mi familia. Particularmente de mi madre Lety Guzmán, ella me ha llenado de motivación cada día de los últimos 4 años y medio para alcanzar este punto y me ha dado las herramientas desde pequeño para afrontar los retos de la vida con valentía y determinación. Este proyecto es nuestro. Agradezco mis hermanas mayores, Mariana y Carolina por ser mi ejemplo a seguir y por depositar su confianza en mí. También a mi padre, Mario por sus consejos y sabiduría.

Agradezco a mis amigos y colegas Ernesto Lora, Gustavo Rodríguez, Uriel Reyes, Christopher Alarcón, Juan Pablo Martínez por acompañarme durante la licenciatura, compartir sus conocimientos conmigo, por trabajar en equipo, por enseñarme a percibir la belleza de la física y las matemáticas, sin duda fueron una parte clave para formarme como físico. Finalmente, a mis amigos de toda la vida Samuel L., Miguel C. y Miguel G. por depositar su confianza y creer en mí. Finalmente, agradezco a la Biotecnóloga Ana por haber sido mi compañera de vida durante los últimos 4 años de la licenciatura, por llenarme de ganas de mejorar, por celebrar conmigo cada paso, estoy muy agradecido por sus consejos, apoyo y por compartir el amor por la ciencia. Gracias a todos por hacerme crecer.

Table of contents

Resume

This work addresses the study of Lipkin-Meshkov-Glick model in order to measure delocalization of the Husimi function through the computation of Wehrl entropy, with the aim of exploring the behaviour of entropy curves that appear around avoided crossings. This phenomenon is observed at the energy spectrum in certain region of the Hamiltonian parameter space.

In chapter 1, it is presented a compilation of previous results and facts, as well as the scope of this work are presented. Among which stands out the Hamiltonian and the particular coupling parameters for which avoided crossings are observed. In chapter 2, the methods and algorithms used to find numerical solutions through programming languages and computation tools are detailed. Finally, in chapter 3, the behaviour of the width of the entropy curves close to avoiding crossings and its relation with the energy difference of consecutive pairs above the so-called Excited State Quantum Phase Transition (ESQPT) are presented.

Introduction

The Lipkin-Meshkov-Glick model is a many-body system that can be studied in a simple form because it can be reduced to a one degree of freedom system. This model can be interpreted as a system of interacting spins, i.e. a many-body system with the advantage of describing a collective behaviour. These kind of systems are subject of interest due to their simplicity and utility to describe quantum systems [1]. In many-body systems interesting phenomena like quantum phase transitions or dynamical tunneling usually appear. Particularly, these phase transitions have been studied using the Lipkin-Meshkov-Glick model [2, 3]; recently, the model has been used to test quantum algorithms designed to calculate nuclear properties using quantum algorithms based on this model [4] and studies of the same have been carried out in presence of Markovian processes of dissipation [5]. The localization and entropy in many-body models is an active research area due to its possible applications on quantum information [6]. Although it is a simple model, it has been used to study quantum phenomena like excited state quantum phase transitions and avoided crossings [7].

In [8, 9, 10] the Hamiltonian is studied in order to distinguish regions of the model parameter space according to classical trajectories and its density of states. Furthermore, a quantum-classical correspondence between classical trajectories and Husimi function is observed . Particularly, in [9], the behaviour of the Wehrl entropy in the vicinity of avoided crossings in the energy spectrum of the Lipkin-Meshkov-Glick model has been studied. It is observed that there exists an increase of the entropy right on the value corresponding to an avoided crossing and a decrease after the crossing.

These avoided crossings take place in pairs of consecutive energy levels at an intermediate energy region delimited by two critical energies associated to what is called an Excited-State quantum phase transition (ESQPT) [11]. A sudden increase in the entropy signalled by a peak is observed upon varying the coupling parameter. The width of these peaks diminishes as the energy of the avoided levels increases. However, until now there are no detailed studies exploring the behaviour of these peaks. When two energy levels present an avoided crossing as a function of some Hamiltonian parameter, there is a superposition

of classical trajectories in the Husimi function of the Hamiltonian eigenfunctions, which in turn, signal that dynamical tunnelling is occurring [12]. In [9] it is demonstrated that the increase of entropy around an avoided crossing is connected with this phenomenon. Then, this work covers the study of Wehrl entropy around the avoided crossings at the energy spectrum as different parameters of the LMG Hamiltonian are varied. Furthermore, the relation between the width of these curves and the energy difference of pairs of states at several avoided crossings are presented.

Avoided Crossings

In Quantum mechanics, the phenomenon of avoided crossings (AC) can be visualized when a pair of eigenvalues associated to a hermitian matrix are constrained to not reach degeneracy, i.e. they approach but "repel" each other at certain values of a parameter in the Hamiltonian. As an example, for a given Hamiltonian $\hat{H}$ and a perturbation $\hat{W}$ the matrix representation of the perturbed Hamiltonian is

$$\hat{H}' = \hat{H} + \hat{W} = \begin{pmatrix} E_1 & 0 \\ 0 & E_2 \end{pmatrix} + \begin{pmatrix} 0 & W \\ W^* & 0 \end{pmatrix} = \begin{pmatrix} E_1 & W \\ W^* & E_2 \end{pmatrix}$$

Through characteristic equation, the eigenvalues of this matrix are given by

$$E_{\pm} = \frac{1}{2}(E_1 + E_2) \pm \frac{1}{2}\sqrt{(E_1 - E_2)^2 + 4|W|^2}$$

Note that if $W = 0$, the solutions are just the diagonal elements of the original Hamiltonian $\hat{H}$ as expected, because it's a diagonal matrix. The effects of some fixed coupling parameters W on the eigenvalues $E_{\pm}$ are shown in figure 1. These two expressions for the eigenvalues $E\pm$ in the previous equation are represented in figure 1 as a function of $\Delta E \equiv (E_2 - E_1)/2$ and $E_{\texttt{mean}} \equiv (E_1 + E_2)/2$; $E_{\pm}$ curves behave as a hyperbola. The main differences in these panels (a)-(d) show up as the coupling parameter W changes. When $W \neq 0$ the E_+ and E_- repel each other or "avoid the crossing". iF $\Delta E = 0$, the energy gap between E_+ and E_- is $2|W|$. If $W = 0$, these levels will cross. A deeper discussion of this example and applications can be found in [13].

Dynamical Tunneling

In the study of Quantum mechanics it is common to deal with potential wells and barriers. The tunnelling phenomenon occurs when a particle's wave function is next to one of these barriers, in this case, the particle acquires a probability of being reflected and being

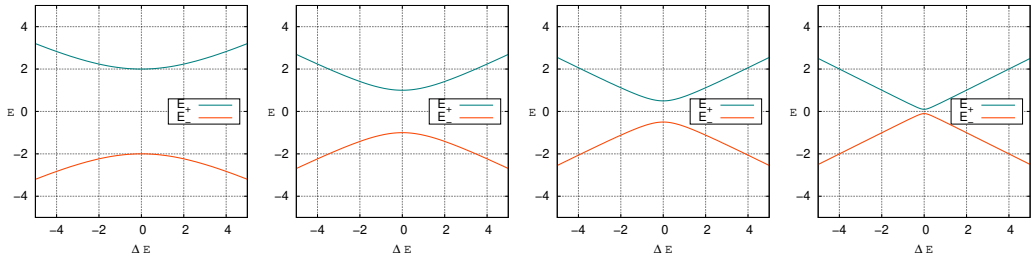

(a) $W = 2$ (b) $W = 1$ (c) $W = 0.5$ (d) $W = 0.1$

Figure 1: Eigenvalues E_+ (green) and E_- (orange) as a function of the energy difference $\Delta E = E_2 - E1$. E_+ and E_- show an approach at 0 that is more significant as the parameter W decreases.

transmitted (in certain cases, it will cross the barrier) [13]. The classical equations of motion pose a barrier rather than a potential function. Particularly, it is possible to observe tunneling even if there's no potential barrier, this class of tunneling is called dynamical tunneling [14] and allows that two (classically) disconnected regions in phase space get connected [12, 15].
The avoided crossing indicates that two levels are interacting. If, in addition, the corresponding classical trajectories to each level pertain to different regions in phase space, then this is a signal that dynamical tunneling is occurring between them. [12].

Excited State Quantum Phase Transition

Usually abbreviated as ESQPT, this concept indicates that exists a critical border or curve in the energy spectrum where a set of excited states exhibit nonuniform variations of the energy as a function of a control parameter. The ESQPT is also identified in regions of non-analytic behavior at the Energy Density of States (EDoS) [11].

1 Theoretical Framework

In this chapter we discuss some basic concepts of the Lipkin-Meshkov-Glick model, as well the theoretical approach to analyse the behavior of the Wehrl entropy around the coupling where avoided crossings occur. In section 1.1 the original Hamiltonian is reviewed, as well as its symmetries and its properties depending on the region of the parameters space. A generic formula to identify avoiding crossing at certain couplings is presented in section 1.2. Previous results related to dynamical tunneling and entropy are discussed in sections 1.3 and 1.5, respectively. In sections 1.4 and 1.6 the theoretical basis concerning to phase space, Husimi function and Excited State Quantum Phase Transition (ESQPT) are reviewed.

1.1 The Lipkin-Meshkov-Glick Model

The Lipkin-Meshkov-Glick (LMG) model was originally proposed in the 1960's in the field of nuclear physics as a model to describe many-body systems. Particularly, the dynamics of N fermions in two N-fold degenerate levels which interact with each other through a monopole-monopole force [16]. In the most general form, LMG Hamiltonian is written in terms of fermionic operators $a^{\dagger}_{p,\sigma}$

$$\begin{aligned}\hat{H}_{LMG} = \frac{1}{2}\epsilon_0 \sum_{p,\sigma} \sigma a^{\dagger}_{p,\sigma} a_{p,\sigma} + \frac{V}{2} \sum_{p,p',\sigma} a^{\dagger}_{p,\sigma} a^{\dagger}_{p',\sigma} a_{p',-\sigma} a_{p,-\sigma} \\ + \frac{W}{2} \sum_{p,p',\sigma} a^{\dagger}_{p,\sigma} a^{\dagger}_{p',-\sigma} a_{p',\sigma} a_{p,-\sigma}\end{aligned} \tag{1.1}$$

where p denotes the state ($p = 1, \ldots, N$) and σ the level ($\sigma = \pm$) [17]. Since this model consists of only two possible levels, the whole system can be considered as a set of spins. Using the SU(2) representation, the Hamiltonian can be reformulated using pseudo-spin operators

$$\hat{J}_{+} = \sum_{p} a^{\dagger}_{p+} a_{p-} \quad ; \quad \hat{J}_{-} = \sum_{p} a^{\dagger}_{p-} a_{p+} \quad ; \quad \hat{J}_{z} = \frac{1}{2} \sum_{p,\sigma} \sigma a^{\dagger}_{p,\sigma} a_{p,\sigma} \tag{1.2}$$

This simplification leads to the following expression

$$\hat{H}_{LMG} = \epsilon_0 \hat{J}_z + \frac{1}{2}V\left(\hat{J}_+^2 + \hat{J}_-^2\right) + \frac{1}{2}W\left(\hat{J}_+\hat{J}_- + \hat{J}_-\hat{J}_+\right) \tag{1.3}$$

where W and V control the particle interactions [16]. Furthermore, it is convenient to introduce a different parametrization, namely

$$\gamma_x = \left(\frac{2J-1}{\epsilon_0}\right)(W+V) \quad ; \quad \gamma_y = \left(\frac{2J-1}{\epsilon_0}\right)(W-V) \tag{1.4}$$

from these equations is straightforward to see that W and V are given by

$$W = \left(\frac{\epsilon_0}{2J-1}\right)\frac{1}{2}\left(\gamma_x + \gamma_y\right) \quad ; \quad V = \left(\frac{\epsilon_0}{2J-1}\right)\frac{1}{2}\left(\gamma_x - \gamma_y\right)$$

substituting these expressions in equation (1.3) it can be reduced to

$$\hat{H}_{LMG} = \epsilon_0\left[\hat{J}_z + \left(\frac{\gamma_x}{2J-1}\right)\hat{J}_x^2 + \left(\frac{\gamma_y}{2J-1}\right)\hat{J}_y^2\right] \tag{1.5}$$

Furthermore, note that operators in equation (1.2) can be written in terms of spin-$1/2$ operators S_{pi} as follows

$$\hat{J}_+ = \sum_p S_{p+} \quad ; \quad \hat{J}_- = \sum_p S_{p-} \quad ; \quad \hat{J}_z = \sum_p S_{pz} \tag{1.6}$$

With this representation, the LMG model can be seen as an interacting model of $N = 2J$ spins where each of them interact in the same way with the others.

$$\hat{H}_{LMG} = \epsilon_0\left[\sum_p S_{pz} + \left(\frac{\gamma_x}{2J-1}\right)\sum_{p,p'} S_{px}S_{p'x} + \left(\frac{\gamma_y}{2J-1}\right)\sum_{p,p'} S_{py}S_{p'y}\right] \tag{1.7}$$

Since the Hamiltonian commutes with $\hat{J}^2$ it can be diagonalized exactly in the basis of eigenstates of angular momentum $|J\, m\rangle$ where $m \in \{-J, -J+1, ..., J-1, J\}$ [9]. For a fixed value of J, the resulting eigenvalues depend on the parameters γ_x and γ_y, this fact allows to define a parameters space and classify each region according to its behavior in phase space. This parameter space of LMG Hamiltonian was first studied in [9, 17, 8] and it is defined according to different regimes that appear at the Energy Density of States (EDoS) which (semiclassically) is given by

$$\rho(E) = \frac{J}{2\pi}\int \mathrm{d}z\mathrm{d}\phi\, \delta[H(z,\phi) - E] \tag{1.8}$$

Where $H(z,\phi)$ is the classical LMG Hamiltonian. Using this equation at region III of parameter space, it is possible to observe a logarithmic divergence situated at vertical dotted line in figure 1.1a.

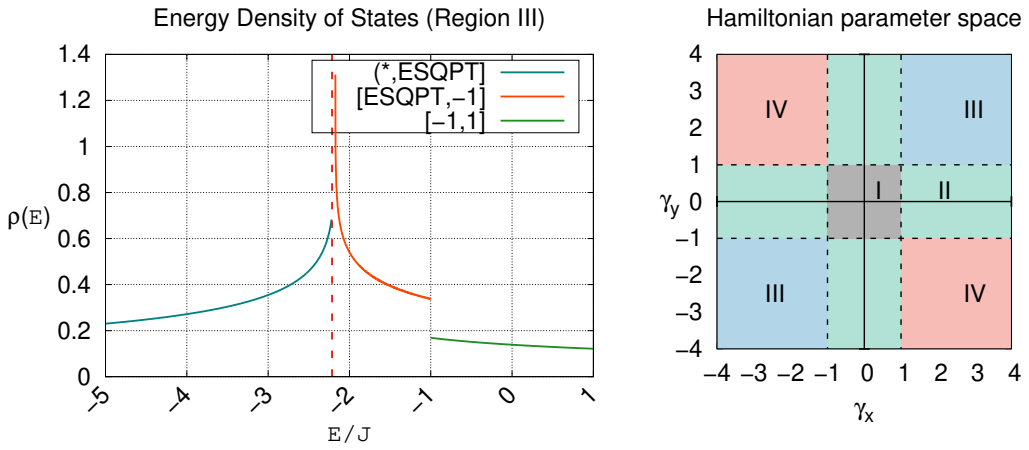

(a) (b)

Figure 1.1: (a) Semiclassical aproximation of the Energy Density of States in region III of the Hamiltonian parameter space (Similar figures as those presented in [9, 17, 8]). Excited State Quantum Phase Transition is a logarithmic divergence.

1.2 Phase Space and Husimi Function

The phase space is a general geometric representation of some system configuration. It takes advantage from generalized coordinates q_j and generalized momenta p_j to define a 2-n dimensional space [18], which is useful to observe the motion of the system. It is convenient in classical mechanics because every instant of motion is well-defined; by contrast, in quantum mechanics, Heisenberg's uncertainty principle does not allow to define simultaneously conjugate variables without uncertainty, then it is not possible to use the same approach. Instead, probability densities plays a fundamental role in describing all the possible states of the system.

This principle also imposes a lower limit (of uncertainty) that lets construct the "most classical" state of the system which leads to quasi-classical results; these kind of states are called coherent states [13]. Particularly, the coherent states of the Bloch sphere were previously used in [9, 8] to analyse the quantum-classical correspondence of trajectories in phase space and Husimi function of LMG model. The spin coherent states or Bloch states are constructed by applying a rotation operator to minimal projection state $|J, -J\rangle$ [8] as shown in the following equation

$$|\alpha\rangle = \frac{e^{\alpha \hat{J}_+}}{\left(1+|\alpha|^2\right)^J}|J,-J\rangle = \frac{1}{\left(1+|\alpha|^2\right)^J}\sum_{m=-J}^{J}\binom{2J}{J+m}^{1/2}\alpha^{J+m}|J,m\rangle \tag{1.9}$$

where $\alpha = \tan(\theta/2)e^{-i\phi}$ is a complex number written in spherical coordinates. On the other hand, the eigenstates of the LMG Hamiltnonian, in general, are given by

$$\left|E_k\right\rangle = \sum_{m=-J}^{J} C_m^k \,|J,\, m\rangle \tag{1.10}$$

Now, the frame is complete to introduce the Husimi function $Q(x,p)$; a practical quasi-probability distribution in the sense that it is always positive but, to integrate Q respect to x or p does not lead to the marginal probability distributions. Nevertheless, this distribution allows the study of the boundaries between quantum and classical mechanics [19]. The Husimi function is defined as the expectation value of some density matrix $\hat{\rho}$ in a basis of convenient coherent-state [20]. When dealing with a pure state of form $\hat{\rho} = \left|E_k\right\rangle\left\langle E_k\right|$ (each one given by (1.10)) it is straightforward to find that Husimi function can be written as the square of the projection of a coherent state and a pure eigenstate of the Hamiltonian as follows

$$Q_k(\alpha) = \left|\langle\alpha\left|E_k\right\rangle\right|^2 \tag{1.11}$$

where

$$\langle\alpha\left|E_k\right\rangle = \frac{1}{\left(1+|\alpha|^2\right)^J}\sum_{-J}^{J} C_m^k\binom{2J}{J+m}^{1/2}(\alpha^*)^{J+m} \tag{1.12}$$

The coefficients C_m^k are determined via diagonalization.

Following the notation used in [9], the Husimi function can be visualized in the Q-P space defining these canonical variables as follows

$$Q = \sqrt{2(1-\cos\theta)}\cos\phi \quad ; \quad P = \sqrt{2(1-\cos\theta)}\sin\phi \tag{1.13}$$

where θ, ϕ (and $\rho = 1$) are the usual variables in spherical coordinates. Furthermore, the Husimi functions can be sorted in ascending order according to the eigenvalues. This allows to assign a k-value to every eigenstate of the Hamiltonian.

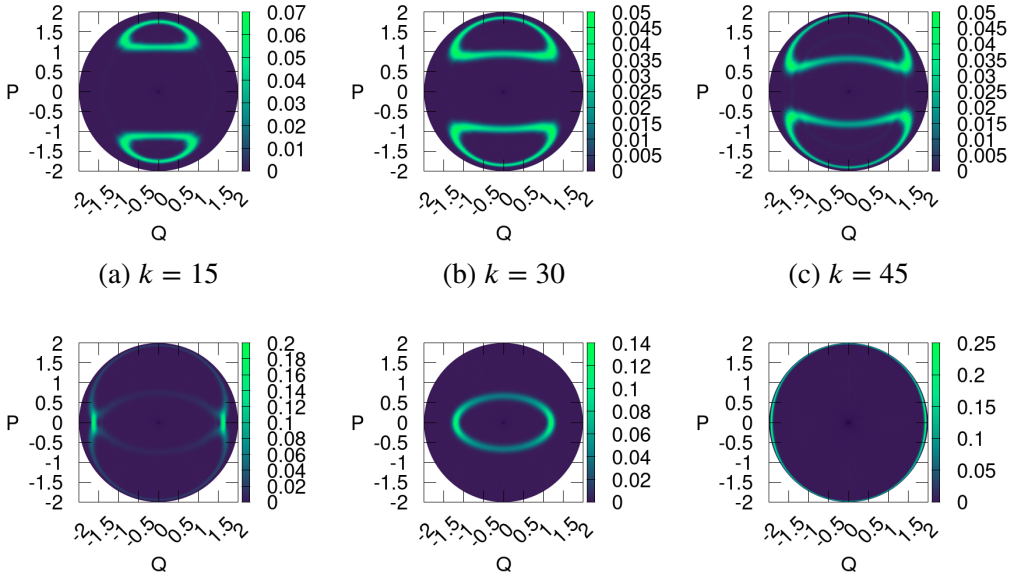

(a) $k = 15$ (b) $k = 30$ (c) $k = 45$

(d) $k = 60$ (e) $k = 75$ (f) $k = 80$

Figure 1.2: Husimi function of eigenstates $|E_k\rangle$ of the positive parity in the Q-P space. $J = 100$, $\gamma_x = -4$, $\gamma_y = 3\gamma_x$.

In figure 1.2, there are examples of the Husimi function for different eigenstates k of the positive parity. In fact, previously in [9, 8], it was shown that the Husimi function of states over all parameter space corresponds to classical trajectories in phase space. Furthermore, these states of the Bloch sphere can be evolved in time following the equation

$$Q(\alpha, t) = \left| \langle \alpha | \hat{U}(t) | \alpha \rangle \right|^2, \tag{1.14}$$

as can be seen in figure 1.3 [9].

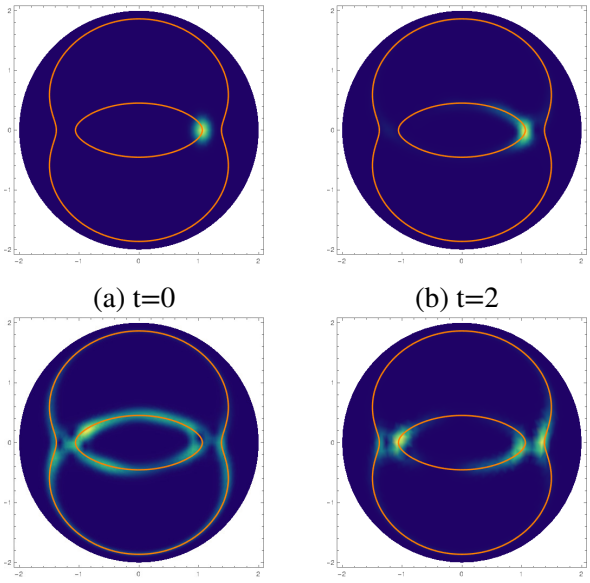

(a) t=0 (b) t=2

(c) t=20 (d) t=200

Figure 1.3: Time evolution of a coherent state for different times and a coupling $\gamma_x = -4.10331$ and $\gamma_y = 3\gamma_x$ [9].

1.3 Avoided Crossings

Theoretically, the latter two terms of the Hamiltonian in equation (1.5) are called perturbations or couplings of the unperturbed Hamiltonian $\hat{H}_0 = \epsilon_0 \hat{J}_z$; when $\gamma_x = \gamma_y = 0$, all particles are placed in the lower level and the energy solutions are just the eigenvalues of $\hat{J}_z$ [16]. The Hamiltonian of equation (1.5) has as solution $2J + 1$ energy levels which depend on coupling parameters; if we define one of these couplings in terms of the other, then it can be visualized the energy as a function of only one parameter.
It is possible to determine the values of coupling parameters for which the energy spectrum exhibits real and avoided crossings. This can be addressed using the Einstein-Brillouin-Keller quantization rule [9], which leads to the following condition

$$\gamma_x \gamma_y = \left[\frac{2J-1}{2J-N}\right]^2 \tag{1.15}$$

where $N \in \mathbb{Z}$ and $0 < N < 2J$. In [9] is presented that for odd values of N, the coupling parameter results in real crossings and for even values of N_e, avoided crossings are obtained. Now, we can introduce the notation γ_x^{AC} to denote the values of the coupling

parameters that indicate the exact position (in double precision) of ACs in the energy spectrum. Particularly in this work, one of the coupling parameters is defined in terms of the other as $\gamma_y = 3\gamma_x$, then equation (1.15) at regime III of the EDoS where avoided crossings takes place is

$$\left|\gamma_x^{AC}\right| = \frac{1}{\sqrt{3}}\left[\frac{2J-1}{2J-N_e}\right]. \tag{1.16}$$

In figure 3.4, $|\gamma_x^{AC}|$ is shown as a vertical dotted line computed with (1.16) and several avoided crossings centered at this value. Additionally, it can be observed that these pairs of states are situated above the excited state quantum phase transition.

1.4 Dynnamical Tunneling

As it was discussed in the previous section, energy spectrum of LMG model presents avoided crossings at certain values of the coupling parameter. In earlier works of Lerma, Nader and González-Rodríguez, it was demonstrated that dynamical tunneling occurs at the exact value where ACs are placed, i.e. there is a superposition of classical trajectories (figure 1.4) [9, 8] which correspond to different regions in phase space. The behaviour shown in figure 1.4 disappears for the next consecutive pairs of states over ESQPT.

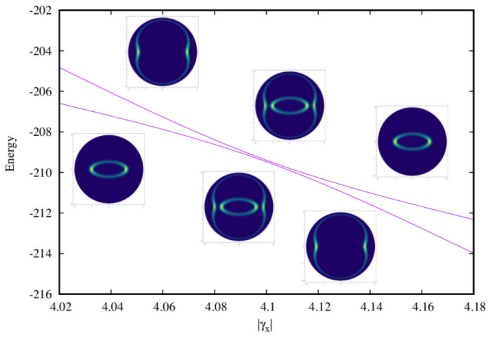

Figure 1.4: There is a superposition of Husimi function at the coupling parameter corresponding to avoided crossings [9].

1.5 Entropy

In the context of Information Theory, entropy is interpreted as lack of information about a system. Then, if we obtain a peak of entropy, the lack of information reaches a maximum.

As previously discussed, in figure 1.4, for the first pair of states over the ESQPT occur a superposition of the classical trajectories right on γ_x^{AC}. For a fixed set of parameters in the Hamiltonian (1.5), the list of eigenvectors is obtained after diagonalization, that allows to calculate the entropy of the eigenstates as function of the coupling parameters. Here Wehrl Entropy will be used as a delocalization measure of the Husimi function, i.e. the lack of information of where a particular eigenstate is localized in phase space is obtained. The Wehrl entropy is defined in terms of the Husimi function as the integral

$$W_E = -\int Q_k(\alpha)\ln Q_k(\alpha)\mathrm{d}\Omega \tag{1.17}$$

where $\alpha = \tan(\theta/2)e^{-i\phi}$ and $\mathrm{d}\Omega = \sin\theta\mathrm{d}\theta\mathrm{d}\phi$ is the solid angle of the unitary Bloch sphere.
In [9], it was observed that this behavior is accompanied with a sudden increase and an interchange of Wehrl entropy centered at the AC. Such curves of entropy disappear for pairs of levels of greater energy.

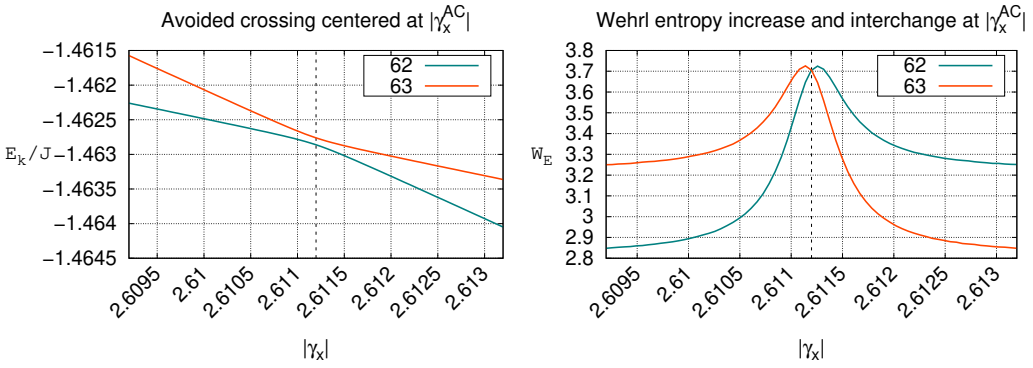

(a) (b)

Figure 1.5: (a) Avoided crossing of the first pair of states after ESQPT for fixed values $J = 100$, $\gamma_x \approx -2.6111$, $\gamma_y = 3\gamma_x$. (b) There is an increase of entropy centered at γ_x^{AC} (vertical dotted line) and an interchange in entropy.

In figure 1.5 the Wehrl entropy of two levels participating in an avoided crossing for couplings close to at γ_x^{AC} is shown. Each level has its corresponding curve of entropy and a peak centered closely to γ_x^{AC}.

1.6 ESQPT in LMG Model

It is of particular interest to study region III of parameter space, i.e. when $|\gamma_x| > 1$, $|\gamma_y| > 1$, $sgn(\gamma_x) = sgn(\gamma_y)$, due to the logarithmic divergence presented at EDoS which also defines Excited State Quantum Phase Transition (ESQPT (See fig. 1.1a) [21]. Furthermore, in [9] it is shown that this ESQPT occurs at an energy given by equation

$$E(\gamma_m)_{\text{ESQPT}} = \frac{\gamma_m + \gamma_m^{-1}}{2} + \text{C} \tag{1.18}$$

where

$$\gamma_M = sgn(\gamma_x) min(|\gamma_x|, |\gamma_y|) \tag{1.19}$$

and

$$\text{C} = \frac{1}{2(2J-1)}\left(\gamma_x + \gamma_y\right) \tag{1.20}$$

Equation (1.18) depends on the coupling parameters. As an example, in figure 1.6 the ESQPT can be visualized in the Energy Density of States for different values of the coupling parameters where ACs occur. In this figure, the Y-axis represents the Energy Density of states determined by the following equation.

$$\rho = \frac{2}{E_{k+1} - E_k} \tag{1.21}$$

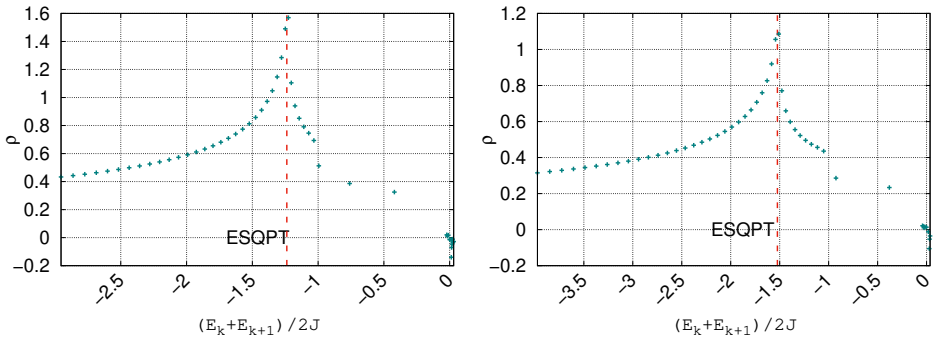

(a) $\gamma_x^{AC} = -1.914878392812259$ (b) $\gamma_x^{AC} = -2.611197808380353$

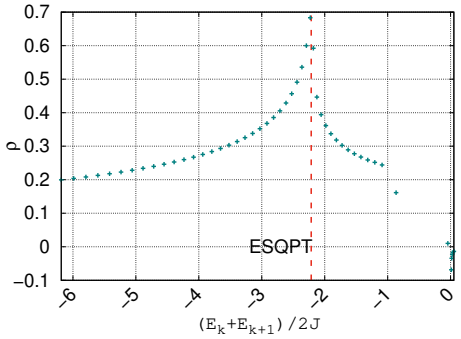

(c) $\gamma_x^{AC} = -4.103310841740555$

Figure 1.6: Energy Density of States. The ESQPT (vertical dotted line) changes as the value of coupling parameters changes. Using equation (1.16) and (1.18) for (a) $N = 140$, (b) $N = 156$, (c) $N = 172$.

2 | Methodology

In this chapter the methods and processes to compute Wehrl entropy will be discussed. Of particular interest is to explore the vicinity around different values associated with avoided crossings and different system sizes. Here, it is discussed how to use this data to analyse the increment of entropy around the corresponding value γ_x^{AC}. Several algorithms are introduced in order to simplify the main problem in basic functions which calculate entropy step by step; these are presented in the section 2.1 and summarised in the flowchart 2.4 in section 2.2. Once Wehrl entropy is obtained, the section 2.3 starts explaining the data analysis and finishes with a review of the particular values and regions explored in this project. Finally, the section 2.4 covers Gaussian curve fitting on Wehrl entropy data points. The discussion of the results and analysis are left to the next chapter.

2.1 Numerical approach

Previously, it was discussed that avoided crossings occur at certain values of the Hamiltoninan coupling parameters; these avoided crossings can be observed in certain regions of the energy spectrum (see figure 2.1), but to observe a considerable amount of AC and the manifestation of the ESQPT, it is necessary to increase the size of the system, i.e. the value J in equation (1.5) must be large enough. Therefore it is necessary to deal with large matrices of dimension $J + 1$ (in the case of positive parity). For this reason, the computational tools are indispensable.

2.1.1 Matrix Representation of LMG Hamiltonian

Equation (1.3) satisfy SU(2) algebra; since we know the action of operators $\hat{J}_\pm$ on the basis $\{|J\ m\rangle\}$, it is straight-forward to show that the matrix elements of the Hamiltonian in this basis can be reduced to the following expression

$$\left\langle J\, m'\right| \hat{H} \left|J\, m\right\rangle = m\delta_{m',m} - \frac{\gamma_x}{2(2j-1)}\Big\{ C_+(J,m)C_+(J,m+1)\delta_{m',m+2} + \\ + C_-(J,m)C_-(J,m-1)\delta_{m',m-2} - 4\big[J(J+1)-m^2\big]\delta_{m',m}\Big\} \tag{2.1}$$

with the following simplifications $\gamma_y = 3\gamma_x$, $\hbar^2 = 1$, $\epsilon_0 = 1$. It is also convenient to define $C_-(J,m)$ and $C_+(J,m)$ (equation (A.3)) to simplify the complete formula. A complete deduction of this equation is treated carefully in appendix A. From this expression, it is possible to obtain the matrix element (m',m) for a particular value of γ_x. As it is mentioned in section 1.3, we consider only the avoided crossings occurring in the sector of positive parity, then we can build the matrix representation of the Hamiltonian (1.5) of dimension $J+1$ where $(m',m) \in \{-J, -J+2, \ldots, J-2, J\}$. Algorithm 1 computes the matrix elements and order them into a 2D array, each iteration computes an element of the matrix for a fixed value of J and particular integers m and m'.

Algorithm 1 Matrix Representation LMG Hamiltonian

```
function HMATRIX(J, γ_x)
    Hmatrix(:, :) := 0                          ▷ Initialize (J + 1) × (J + 1) array
    for m' := −J, J, 2 do                       ▷ Step size: 2
        for m := −J, J, 2 do
            Hmatrix(m', m) = ⟨J m'| Ĥ |J m⟩      ▷ Eq (2.1)
        end for
    end for
    return Hmatrix
end function
```

First of all, it is necessary to observe the energy spectrum (eigenvalues) in the region of interest. As mentioned in section 1.1, region III of EDoS exhibits a logarithmic divergence in the energy density of sates, which defines ESQPT. Then, we must identify which levels present avoided crossings. These have a lower-bound at ESQPT (eq. (1.18)) and an upper bound at $-1+C$ (eq. (1.20)). In addition, we must know the corresponding level numbers k, in order to obtain energy and eigenvectors. In figure 2.1 we can see an example of the energy spectrum and the bounds (blue and red lines) enclosing the region with ACs.

2.1.2 Diagonalization

In order to diagionalize the LMG Hamiltonian, Wolfram Mathematica built-in functions were chosen; these are called *Eigenvalues[]* and *Eigenvectors[]* which take a 2D-array

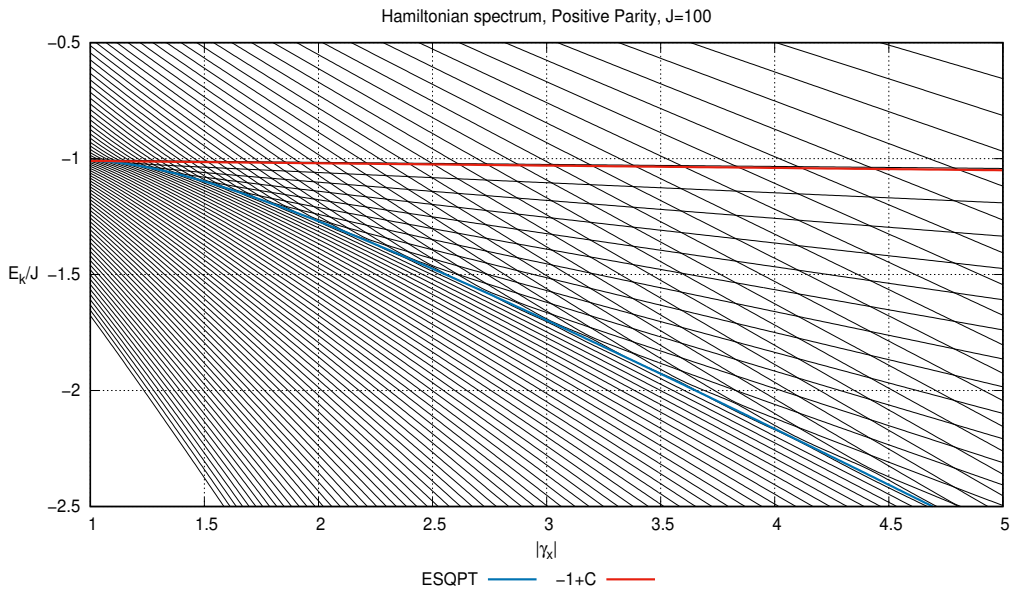

Figure 2.1: Lower and upper bound enclosing energy levels which exhibit avoided crossings.

(square matrix) and computes either symbolic or numerical solutions (more efficient), the output of these functions is a list of the $J + 1$ eigenvalues at γ_x and a list of lists, each one containing the coefficients of the linear combination of the eigenvectors of the LMG in the basis of eigenvectors of $\hat{J}^2$ and $\hat{J}_z$. During the numerical analysis, it was proposed to observe the energy difference of all consecutive levels of the positive parity in high precision for a fixed value of J and γ_x^{AC}. Since the smaller difference is around 1×10^{-35}, it is necessary to increase diagonalization precision to at least 40 digits in order to observe the correct behaviour. The diagonalization of the positive parity matrix for $J = 100$ gives $100 + 1$ energy levels which can be sorted in ascending order, each consecutive pair is shown in the x-axis of figure 2.2. This figure also shows an exponential decrease pattern of the energy gap for avoided crossings as a function of the mean energy of the pairs of levels involved in the ACs.

Most of programming languages does not offer the option to arbitrarily increase the precision of variables, but in Mathematica this was addressed easily using *N[*Hmatrix*,40]*. The purpose of this work is to observe the behaviour of the Wehrl entropy around ACs as the parameters of the Hamiltonian change. It was chosen to export eigenvalues and eigenvectors from Wolfram Mathematica and analyse it in Fortran 90 using double precision (16 digits) for the first seven pairs of states which exhibit ACs. In certain cases, these seven

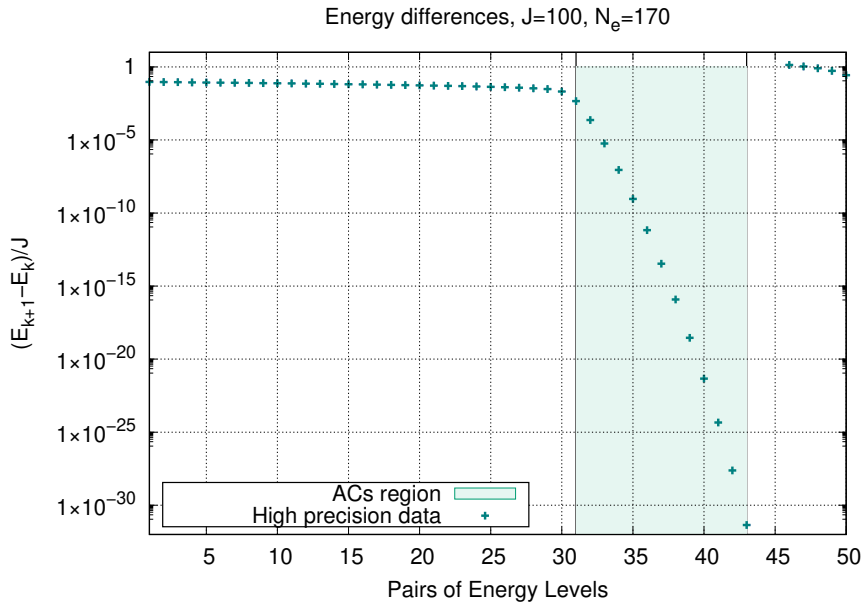

Figure 2.2: Green region shows an exponential decrease in the energy gap of avoided crossings at $|\gamma_x^{AC}|$. In order to be able to detect the small gap for larger energy ACs, high numerical precision was used during diagonalization.

pairs are enough to cover all the region but when γ_x^{AC} is larger, there are more pairs of states with avoided crossings which require more than 16 digits.

Before calculating the entropy, it is necessary to take into account some considerations in order to optimize the computation and obtain the complete behaviour of the entropy around the value of the AC. First, it is recommended to identify visually the pairs of levels which exhibit ACs in the energy spectrum; then we must select the appropriate interval that delimits completely the region of interest (before AC, exact value of AC in double precision and after AC) and make a partition with small enough steps for the coupling parameter. There is not an automated procedure to identify the size of the steps in the relevant interval around the avoided crossings. In [9], it was reported that exists a sudden increase in Wehrl Entropy right on γ_x^{AC} that attenuates for each pair of levels of greater energy, preserving the interchange in entropy. With the increase of precision in diagonalization, it is expected to observe not only the interchange but also peaks of entropy centered at the ACs. However, in order to see that, we shall take smaller steps of the coupling parameters for levels with larger energy.

2.1.3 Monte Carlo Integration

An essential part of the entropy computation consists of evaluating the Husimi function and integrating numerically the equation (1.17). A popular method of integration is Monte Carlo, which is based on random sampling of functions and a large number of iterations. In the simpler case, there is a function $f(x)$ which we want to integrate over the $[a, b]$ interval; following this method, we take a sample of n random points x_i within the interval and the integral is approximated by the average as in the next expression.

$$I = \int_a^b f(x)\, dx \approx \frac{(b-a)}{n} \sum_{i=1}^{n} f(x_i)$$

It is straight forward to generalize this method to evaluate integrals in more than one dimension. But we must ensure that the size of the sample n is large enough to reach the desired precision. Particularly, in this work, it is required to perform the integration of a function in spherical angles, i.e.

$$I = \int_c^d \int_a^b f(x, y)\mathrm{d}x\mathrm{d}y = \int_0^{2\pi} \int_0^{\pi} f(\theta, \phi) \sin\theta \mathrm{d}\theta\mathrm{d}\phi \tag{2.2}$$

as it is expected, this integral also requires a sample of n points (θ_i, ϕ_i) where $\theta_i \in [0, 2\pi]$ and $\phi_i \in [0, \pi]$, then we shall evaluate the next expression

$$I \approx \frac{(2\pi)(\pi)}{n} \sum_{i=1}^{n} f(\theta_i, \phi_i) \tag{2.3}$$

For the case of interest, we replace $f(\theta, \phi)$ by (1.17), leading to

$$\begin{aligned} W_{E_k} &= -\int_0^{2\pi} \int_0^{\pi} Q_k(\alpha)_k \ln\left(Q_k(\alpha)\right) \sin\theta \mathrm{d}\theta\mathrm{d}\phi \\ &\approx \left(\frac{2\pi^2}{n}\right)\left(\frac{2J+1}{4\pi}\right) \sum_{i=1}^{n} Q_k(\theta_i, \phi_i) \ln\left(Q_k(\theta_i, \phi_i)\right) \sin\theta_i \end{aligned} \tag{2.4}$$

where a normalization factor $\left(\frac{2J+1}{4\pi}\right)$ has been introduced. In order to simplify the main ideas of the algorithm to compute the Wehrl Entropy (equation (2.4)), two important algorithms are analysed. The function in algorithm 2 requires the size of the system J, a particular value of θ and ϕ, as well as the k-th eigenvector E_k of LMG Hamiltonian (this is a list of coefficients). Before starting the cycle, we must initialize a complex variable *sum* and fix the value of $\alpha(\theta, \phi)$. The output of this algorithm is Q, i.e Husimi function evaluated at (θ, ϕ) (a real number).

Algorithm 2 Evaluate Husimi function

```
1:  function HUSIMI(J, E_k, θ, φ)
2:      sum = 0 + 0i                                  ▷ Initialize a complex number
3:      α = tan(θ/2) e^{-iφ}
4:      for i := −J, J, 2 do
5:          b = binomial(2J, J + i)
6:          sum = sum + (b)^{1/2} E_k(i)(α*)^{J+i}    ▷ Sum in eq. (1.12)
7:      end for
8:      h = 1/(1 + |α|^2)^J                           ▷ Quotient in eq. (1.12)
9:      Q = |h × sum|^2                               ▷ Eq. (1.11)
10:     return Q                                      ▷ Real number
11: end function
```

Now an algorithm is necessary to evaluate the Husimi function over a region of the form

$$\{(\theta, \phi)|0 \leq \theta \leq \pi\,;\, 0 \leq \phi \leq 2\pi\} \tag{2.5}$$

Algorithm 3 summarizes the construction of Husimi function sample over this interval. At each iteration Husimi() is called to determine the value of $Q(\theta, \phi)$, eq. (1.11). This value is used to compute the argument of sum in equation (2.4), this is one of the n evaluations to perform the integration by Monte Carlo; each of them are stored in a list called *values()* that will be used to integrate numerically.

As we have already stored all the evaluations in this list, we only have to select randomly the elements of *values()* and sum them a large number n of times and then multiply by the two quotients written in the left side of equation (2.4). Since this step is easy to perform we will assume the function MonteCarlo() in algorithm 4, where the output of this function is simply the result of equation (2.4), i.e. Wehrl entropy of E_k at γ_x.

2.2 Entropy algorithm

Now, the algorithm to compute Wehrl entropy is introduced. For a particular value of J, γ_x and an eigenvector E_k, a Wehrl entropy value is calculated at each iteration of algorithm 4, where each integration requires a number of iterations (n). The purpose of this algorithm is to automate the computation for appropriate interval of the coupling parameter $\{\gamma_{xi}\}$ around γ_x^{AC} and a pair of consecutive eigenvectors $\{E_k, E_{k+1}\}$ in the regions of interest. In addition, it is convenient to emphasize that each pair of states of greater energy require a different interval of γ_x because the interval is significantly smaller. Since there is no

Algorithm 3 Sample of points

```
1:  function SAMPLE(J, E_k)
2:      Values(:) = {0.0, ..., 0.0}
3:      Δ = π/100
4:      θ = 0
5:      aux = 1
6:      for i := 0, 100 do
7:          φ = 0
8:          for j := 0, 200 do
9:              Q = Husimi(J, E_k, θ, φ)              ▷ Q(α), algorithm 2
10:             values(aux) = Q sin(θ) ln(Q)          ▷ argument (2.4)
11:             aux = aux + 1
12:             φ = φ + Δ
13:         end for
14:         θ = θ + Δ
15:     end for
16:     return values                  ▷ Sample of points in the region 2.5
17: end function
```

information about the width decrement rate, we must propose intervals in an empirical way; that is, after computing Wehrl entropy around γ_x^{AC} we visualize if there are points showing the increase and decrease around γ_x^{AC} and decide if there's need of recalculate the curves. Figure 2.3 shows the consequence of choosing the same interval for consecutive pairs. In this particular case, in the left panel we observe the complete behaviour but we must take smaller interval and steps to recalculate right side figure.

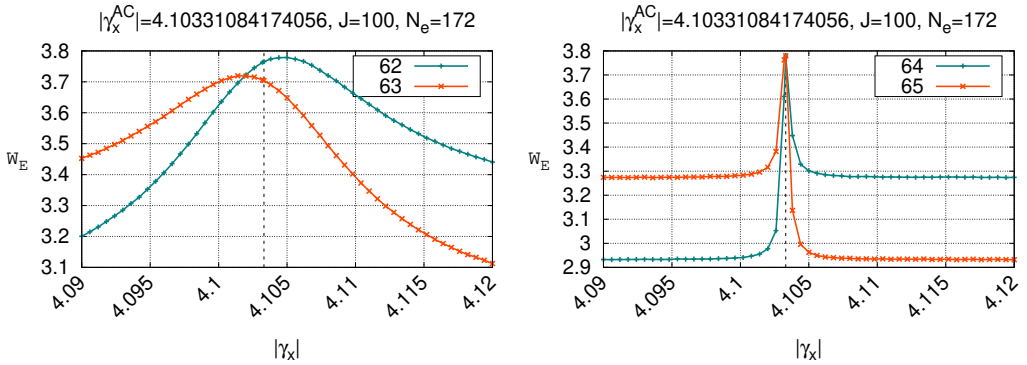

Figure 2.3: Wehrl entropy of two consecutive pairs of levels which exhibit avoided crossings for a fixed value of $J = 100$. Both figures have the same γ_x range but the right one requires smaller steps in order to see a similar behaviour to that on the left. An acceptable result of $k = 64, 65$ is presented in figure B.4c.

2.2.1 Case 1: J fixed

For a fixed value of J, there is a wide number of avoided crossings along the energy spectrum (see 2.1). As the first case, we will choose different ACs and study Wehrl entropy of consecutive levels around each value of γ_x^{AC}. This task is accomplished using equation (1.16), which requires even numbers N_e such that $|\gamma_x| > 1$, $|\gamma_y| > 1$, $sgn(\gamma_x) = sgn(\gamma_y)$ (region III of EDoS).

2.2.2 Case 2: Different J

As we increase the size of the system, the energy density increases i.e. there are more levels in any zone of the energy spectrum and the avoided crossings are shifted to different values of γ_x. Thus, it is not possible to fix the exact same value of the coupling parameter for avoided crossing at different values of J. However, we can choose a similar value and analyze the Wehrl entropy for consecutive pairs after ESQPT around γ_x^{AC}. In equation (1.16), we must find the value N_e for a desired value of J such that the outputs of γ_x are similar. This value must satisfy the constraint discussed in previous case, i.e. it must be at region III.

Algorithm 4 is a general case to compute Wehrl entropy through Monte Carlo integration (using a large number "n" to compute (2.4)) of two consecutive levels and a certain γ_x interval. This process will be used in both cases for each pair involved in avoided crossings.

Algorithm 4 Wehrl entropy around γ_x^{AC}

```
1: function WEHRL(J, n, {E_{k,i}}, {E_{k+1,i}}, {γ_{xi}}, i = 1, 2, ..., r)
2:     for p := k, k + 1 do
3:         for i := 1, r do                                  ▷ r: interval size
4:             evec = E_{p,i}                  ▷ Temporal location of eigenvector
5:             values = Sample(J, E_{p,i})                       ▷ Algorithm 3
6:             Wint = MonteCarlo(values(:), n)                     ▷ Eq. (2.4)
7:             Write: γ_{xi}, Wint                                 ▷ .dat file
8:         end for
9:     end for
10:    return Wehrl.dat                          ▷ Table of points (γ_x, W_E)
11: end function
```

In figure 2.4, the complete process that summarises the algorithms in this chapter is presented. The input is expected to be a fixed J, the γ_x interval of choice and the pair of levels $k,\ k+1$ after ESQPT. Furthermore, it is important to notice that algorithm 4 contains algorithm 3 and 2, then we only call the former to compute the Wehrl entropy of a pair of states. This whole process is repeated for every pair in the levels range presented in tables 3.1 and 3.2. Since eigenvalues and eigenvectors depend on the coupling parameter γ_x, each point (γ_x, W_E) requires to perform all previous steps. That's why it is important to choose an appropriate γ_x range; for larges values of J, the time of diagonalization increase and an inappropriate range will not show the curves of entropy, just a jump centered at γ_x^{AC}.

2.3 Data Processing

The output of algorithm 4 is a table of Wehrl entropy points of the form (γ_x, W_E) which correspond to a pair of levels $k,\ k+1$. If the interval of choice shows a complete behaviour (increase, interchange and decrease); then, this curves are candidates to perform a Gaussian fit on the data, but first we must split it. For a particular pair of levels (see figure 2.5), there are two data tables which describe the purple and green curves 2.5a. First step of processing consist in split the data in "*upper*" and "*lower*". We take the avoided crossing γ_x^{AC} as a reference point (vertical dotted line). From left to right, we take all the points corresponding to upper curve and we merge them with those points of the upper curve to the right of γ_x^{AC}. The same procedure is done with the lower points, resulting two data tables which visualize as figure 2.5b.

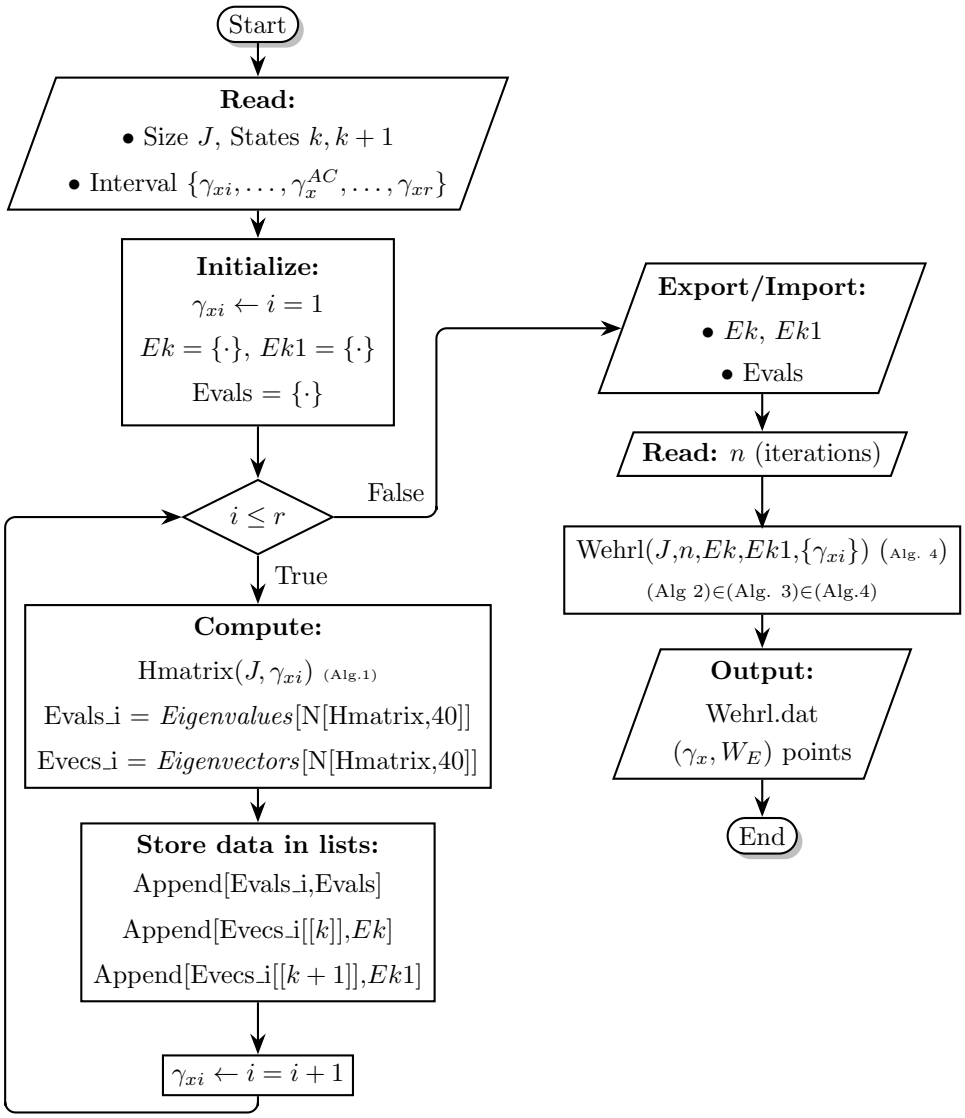

Figure 2.4: Flowchart to compute Wehrl entropy of a pair of states k, $k+1$ around γ_x^{AC}.

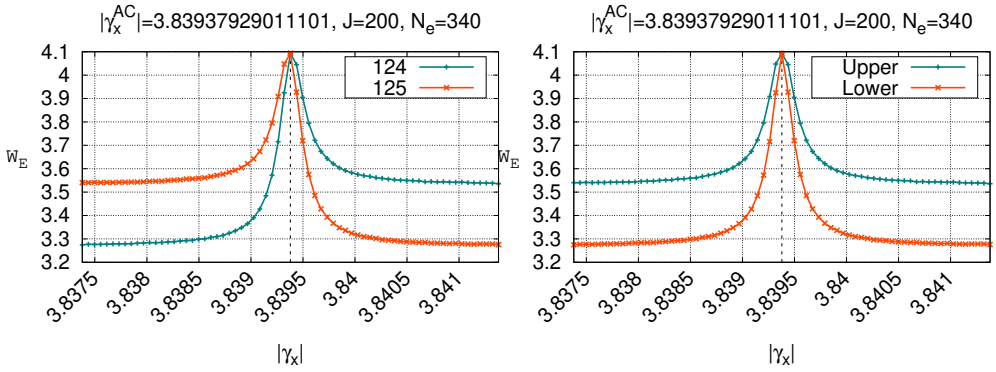

(a) Acceptable output of algorithm 4. (b) Data after split.

Figure 2.5: Data transformation

2.4 Gaussian Fit

By using the built-in function *fit* of the interactive visualization package *gnuplot 5.2*, we fit a Gaussian function to the numerical data. The function has the following form

$$f(\gamma_x) = C + \frac{c}{\sigma\sqrt{2\pi}} \exp\left\{ -\frac{(\gamma_x - |\gamma_x^{AC}|)^2}{2\sigma^2} \right\}, \tag{2.6}$$

where C, c, σ are fitting parameters. In figure 2.6a, they are represented in a simple curve with the form of equation (2.6). C shift the reference of the Gaussian curve with respect to zero, σ control the width of the Gaussian, c is part of the factor $\frac{c}{\sigma\sqrt{2\pi}}$ which measures the amplitude of Gaussian curve respect to C. For a pair of entropy curves (upper an lower) two outputs of fit parameters are obtained (σ_{upper} , σ_{lower} and so on), each one with its error associated ΔC, Δc, $\Delta\sigma$. These values were taken into account to determine

$$\bar{\sigma} \equiv \frac{\sigma_{\text{upper}} + \sigma_{\text{lower}}}{2}. \tag{2.7}$$

A concrete example of some entropy curves after processing, is presented in figure 2.5b and 2.6b.

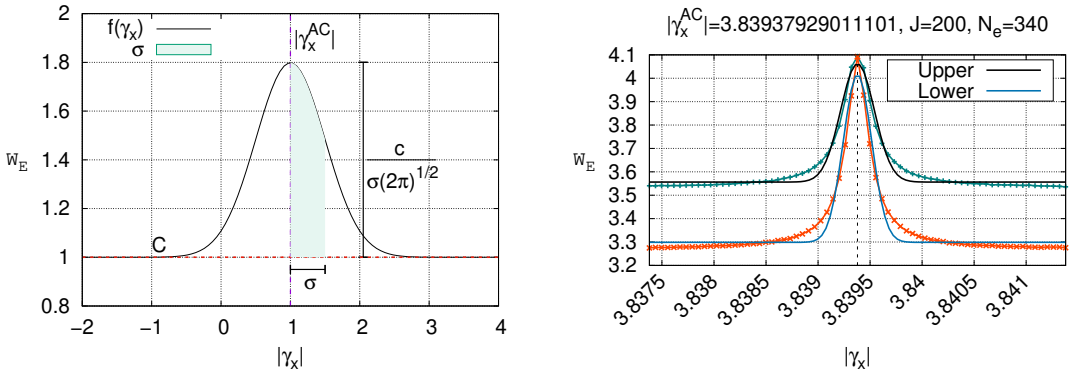

(a) Visualization of parameters. $C = 1$, $c = 1$, $\sigma = 0.5$

(b) Gaussian fit example on data given in figure 2.5b

Figure 2.6: Fitting parameters and example of Gaussian fit.

3 | Results

In this chapter, the results of applying algorithms and methods described in chapter 2 are presented, following the sequences described at the end of the chapter. Particularly, the Wehrl entropy for several avoided crossings was studied (table 3.1) with the size of the system fixed at $J = 100$ (Case 1). Then, for approximately the same value of an AC, we repeated the analysis for larger values of the system size, namely $J = 100,\ 200,\ 500$ (Case 2). The values at these sizes are listed in table 3.2. In section 3.4, the results for the width of the Wehrl entropy peak around avoided crossings, parameter $\bar{\sigma}$, and its behaviour as the energy increases are presented. In section 3.5, the energy gap ΔE at ACs and its behaviour as the energy increases are presented. It was found that these quantities, $\bar{\sigma}$ and ΔE, are linearly correlated.

3.1 Wehrl Entropy around Avoided Crossings

3.2 Case 1

In order to study the Wehrl entropy at several avoided crossings, the size of the system to $J = 100$ was fixed. Then, equation (1.16) was used to find ACs along the energy spectrum. Figure 3.1 shows some of the regions studied here. Table 3.1 shows the list of values obtained in double precision for several avoided crossings, as well as the range of energy levels above the ESQPT which were analyzed. There are certain levels over these ranges which also exhibit avoided crossings but the precision needed to observe superposition on the Husimi function is larger than double precision (16 digits) and at least 40 digits are necessary to observe an increase of the Wehrl entropy for the latter levels below the upper bound $-1 + C$, shown in figure 3.1. Furthermore, it was observed that the first pair of energy levels after ESQPT always show a difference of entropy at γ_x^{AC}, i.e. both entropy curves increase but they don't cross at γ_x^{AC}, this cross appears until the next pair.
Figure 3.2a shows the orange region marked in figure 3.1, where the levels $k = 48,\ 49$ are the lowest pair of energy levels (after ESQPT), see Figure 3.2b whose exhibit a gap

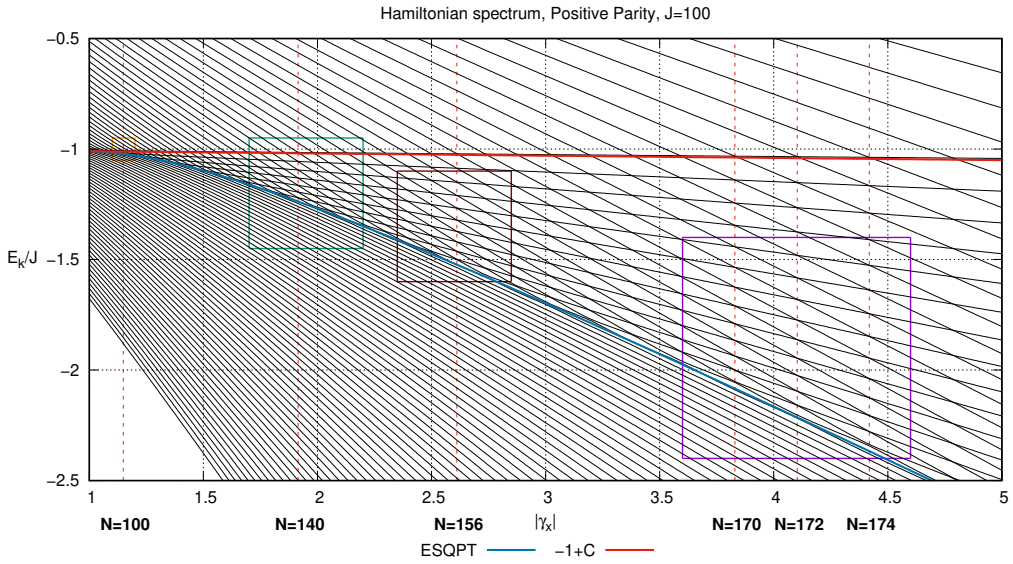

Figure 3.1: Vertical dotted lines denote various γ_x^{AC} along the energy spectrum.

N_e	$\lvert\gamma_x^{AC}\rvert$	Levels
100	1.148927035687355	48-51
140	1.914878392812259	58-69
156	2.611197808380353	60-73
170	3.829756785624518	61-74
172	4.103310841740555	62-75
174	4.418950137259059	61-74
186	8.206621683481109	63-76
196	28.72317589218388	64-77

Table 3.1: Avoided crossings for $J = 100$.

J	N_e	$\lvert\gamma_x^{AC}\rvert$	Levels
100	170	3.829756785624518	61-74
200	340	3.839379290111011	120-132
500	850	3.845152792802908	301-312

Table 3.2: Avoided crossings for different system sizes.

of energy at the AC. Similarly, the next pair given by $k = 50, 51$ and the Wehrl entropy of these levels is given by figure 3.2c, this pair exhibits a cross of the entropy at AC. Analogously, figure 3.3 shows the results for $N_e = 156$, where the crossing of entropy in figure 3.3c occurs at $\gamma_x^{AC} \approx -2.611$, this behaviour is similar for the rest of pairs. The rest of results for all values of N_e shown in table 3.1 and the first two pairs of states are shown in Appendix B.

3.3 Case 2

As the size of the system increases, the Husimi function is more localized in the regions corresponding to classical trajectories. Since the value of the coupling where the avoided crossing occur depends on the size of the system J and on even numbers N_e, it is not possible to have avoided crossing at the same coupling for different system sizes. Nevertheless, it is possible to take similar values for γ_x^{AC}'s. Table 3.2 shows the values of these in the double precision used for studying the entropy as the energy difference respect to the ESQPT critical energy increases. Similar to previous section, in figure 3.4, some levels which exhibit ACs are shown.
Note that the row of table 3.2 was computed in previous section. Entropy curves for $J = 100$, $N_e = 170$ are shown in figure B.3 (Appendix B). Using the next values shown in table 3.2, the entropy of seven pairs after ESQPT were calculated for each J. The results of entropy were similar. As we have seen in previous section, figure 3.5a shows entropy peaks at γ_x^{AC}. It is important to emphasize that the behaviour of energy levels participating in the first avoided crossing above the ESQPT critical energy is peculiar and for that reason, these avoided crossing were excluded of the analysis to obtain $\bar{\sigma}$ and no Gaussian fitting with equation (2.6) was performed for these levels.

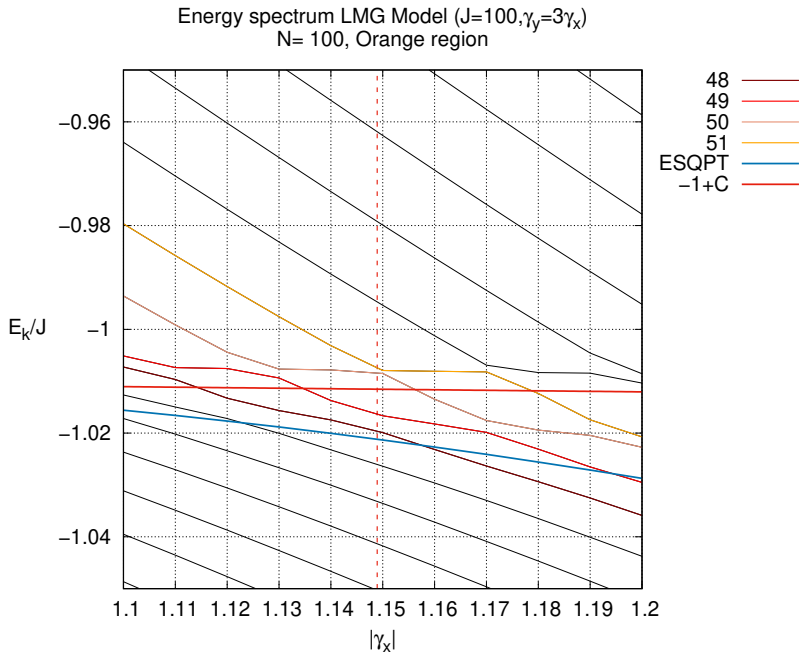

(a) There are only two pairs in this region.

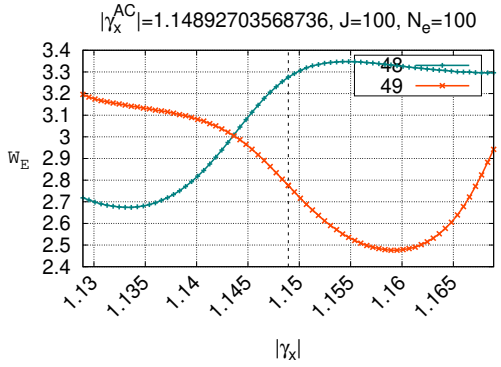

(b) 1st pair show an entropy gap at γ_x^{AC}

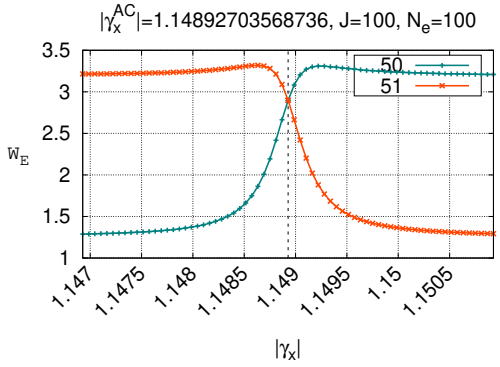

(c) 2nd pair shows a entropy crossing at γ_x^{AC}

Figure 3.2: Werhl entropy of the first two pairs of states after ESQPT for fixed values $J = 100$, $N_e = 100$.

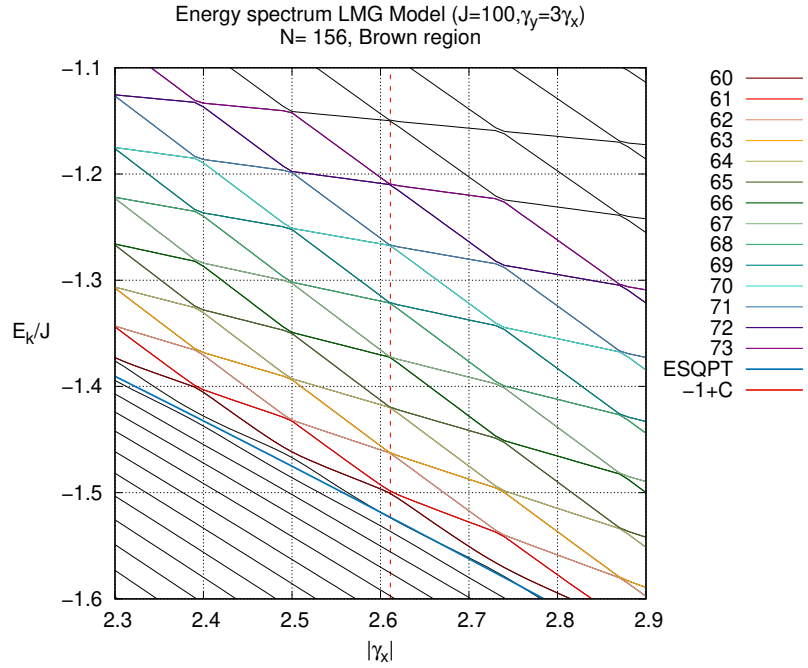

(a) 7 pairs after ESQPT.

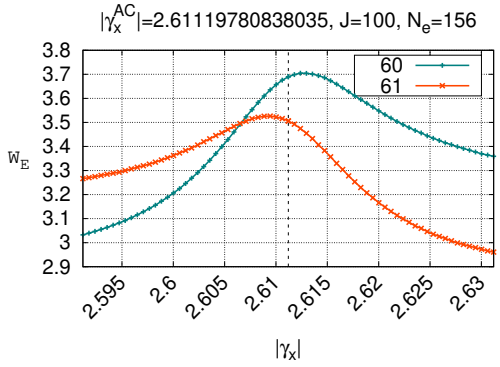

(b) Entropy gap at γ_x^{AC}

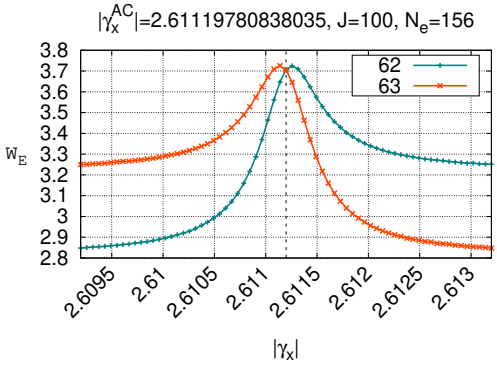

(c) Entropy crossing at γ_x^{AC}.

Figure 3.3: Werhl entropy of the first two pairs of states after ESQPT for fixed values $J = 100$, $N_e = 156$.

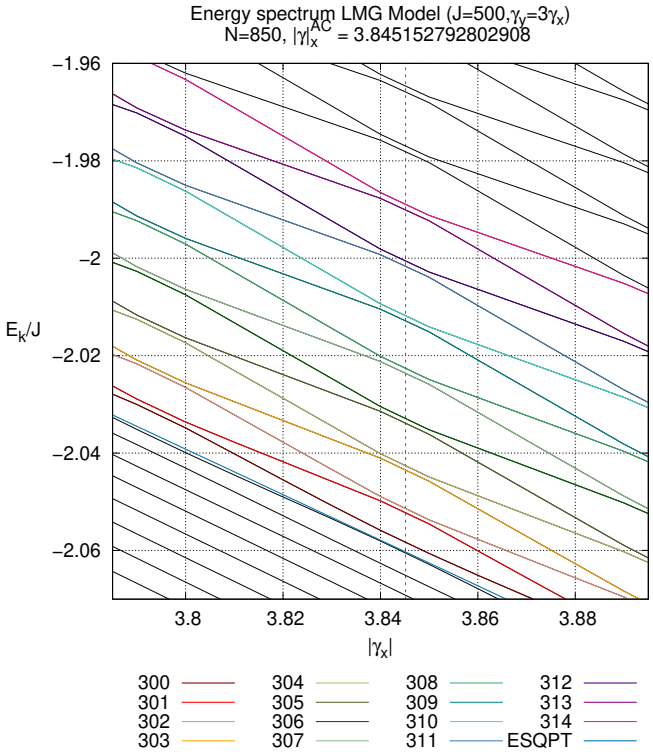

Figure 3.4

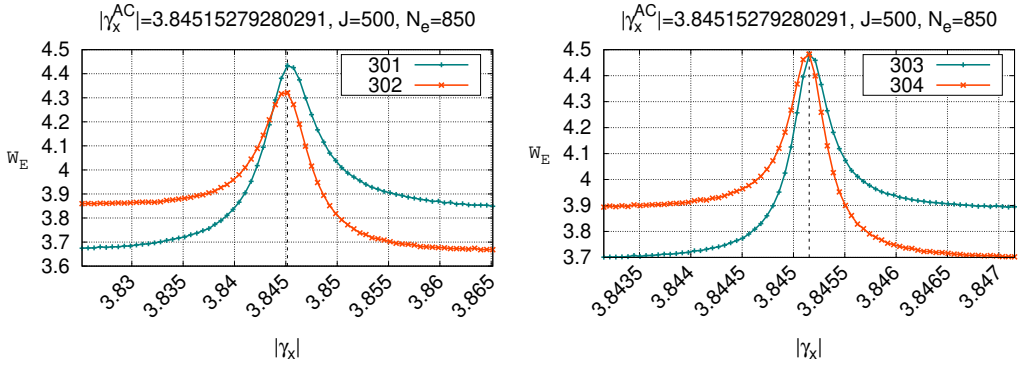

(a) 1st pair after ESQPT.

(b) 2nd pair after ESQPT

Figure 3.5: Wehrl entropy of the first two avoided crossings after the ESQPT critical energy for fixed values $J = 500$, $N_e = 850$.

3.4 Parameter $\bar{\sigma}$ of Gaussian Fits

For every pair of entropy curves (after the 1st pair above the ESQPT critical energy) it was fitted with a Gaussian function of the form of equation (2.6). Figure 3.6 shows an example. As it was described in section 2.4, for each two entropy curves, two parameters were obtained, σ_{upper} and σ_{lower}, which are slightly different but they are at the same order of magnitude. It was observed that the order of this parameter drastically decrease for the next pair of states at higher energy.

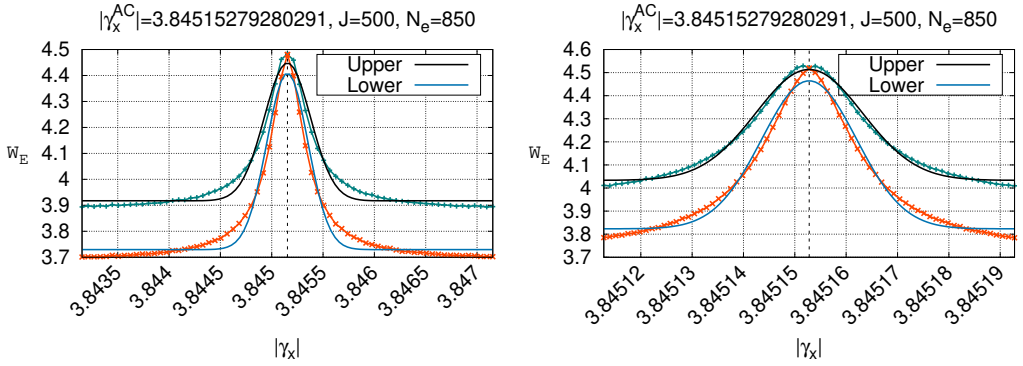

(a) $k = 303, 304$. (b) $k = 305, 306$

Figure 3.6: Gaussian fit on 2nd and 3rd pair after ESQPT for fixed values $J = 500$, $N_e = 850$. Note that γ_x range of panel (b) is smaller.

Since every pair are quasi-degenerated at γ_x^{AC}, there exists an energy gap ΔE and a mean energy $E_{N(\text{mean})}$ for each pair. Here we use these as reference values. In figure 3.7 and 3.8, the behaviour of $\bar{\sigma}$ as a function of the difference $(E_{N(\text{mean})} - \text{ESQPT})/J$ is presented, where ESQPT denotes the ESQPT critical energy of equation (1.18) at γ_x^{AC}. As this difference increases and we take states far from the ESQPT, the width parameter $\bar{\sigma}$ decreases rapidly, then Y axis in both figures are presented in logarithmic scale to observe its behaviour properly. Solid lines are exponential fittings of the form

$$\bar{\sigma} = Ae^{-\alpha(E_{\text{mean}} - \text{ESQPT})/J} \tag{3.1}$$

where A and α are fit parameters. Each line corresponds to only 6 pairs of states starting from the second pair after the ESQPT. We are limited by the double precision to explore pairs of energy levels at higher energies.

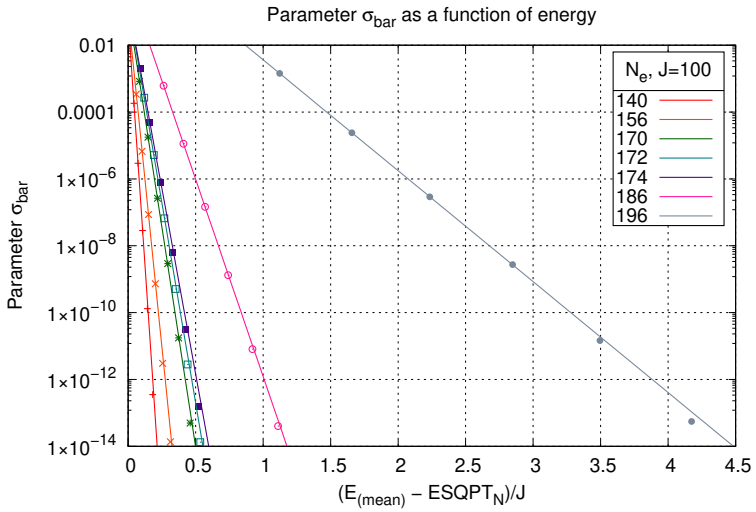

Figure 3.7: Parameter $\bar{\sigma}$ in logarithmic scale as a function of $(E_{\text{mean}} - \text{ESQPT})/J$ for different avoided crossings. $\bar{\sigma}$ decreases exponentially.

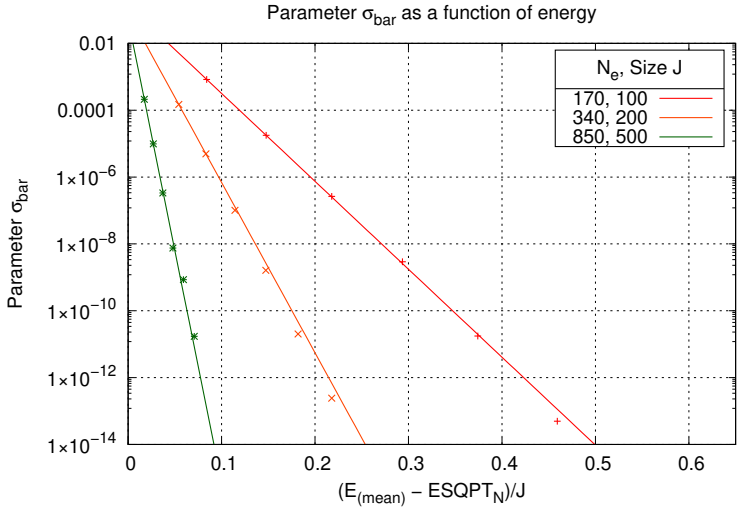

Figure 3.8: Parameter $\bar{\sigma}$ for different system sizes. $\bar{\sigma}$ decreases exponentially.

3.5 Energy gap ΔE at AC

On the other hand,the energy gap of the avoided crossing ΔE (at γ_x^{AC}) as a function of the difference $(E_{N(\text{mean})} - \text{ESQPT})/J$ was also studied. Figure 3.9 and 3.10 show both cases.

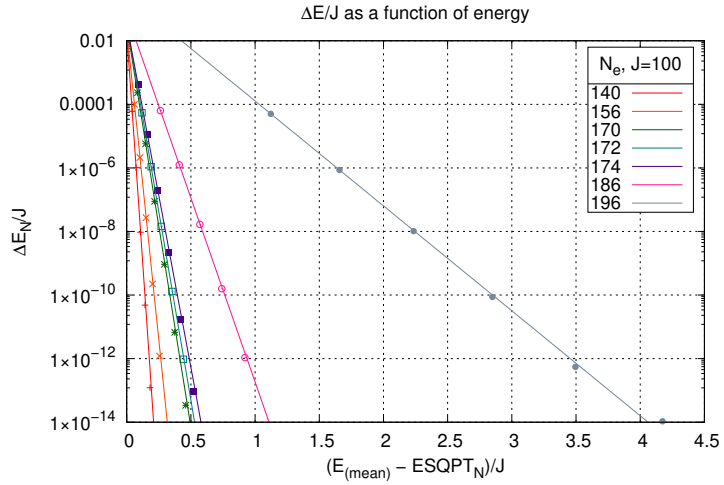

Figure 3.9

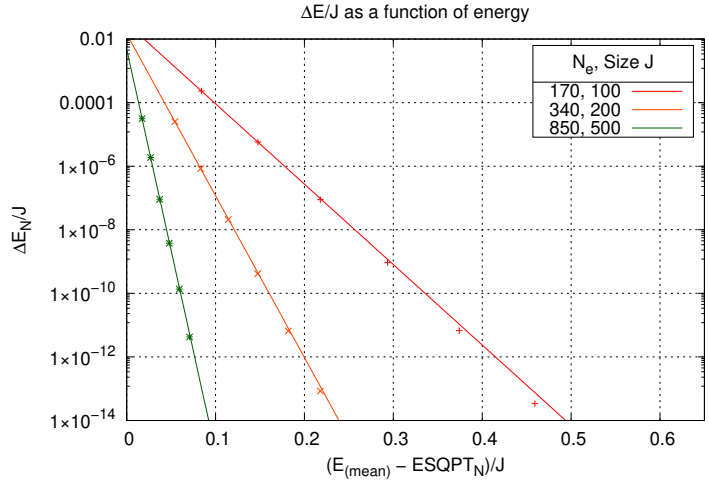

Figure 3.10

Here, solid lines denote an exponential fit of the form

$$\Delta E/J = Be^{-\beta(E_{\text{mean}}-\text{ESQPT})/J} \tag{3.2}$$

where B and β are fit paremeters. In both cases, gap decreases exponentially as we move away from ESQPT.

3.6 $\bar{\sigma}$ and ΔE Correlation

In order to establish the relation between the energy gap of the avoided crossing and the width of the peak in the Wehrl entropy, in figure 3.11, the logarithm of $\bar{\sigma}$ as a function of the logarithm of the energy gap ΔE is plotted for different γ_x^{AC} and a fixed size of the system $J = 100$, whereas in figure 3.12 the same quantities are plotted but for different system sizes ($J = 100, 200$ and 500) and similar coupling parameters γ_x^{AC}. In fact, from equation (3.1) and (3.2), it is possible to show that

$$\ln \bar{\sigma} = m \ln (\Delta E/J) + b, \tag{3.3}$$

where m and b are constants given by $m = \frac{\alpha}{\beta}$ and $b = \ln \frac{A}{(B^{\alpha/\beta}}$. The previous relation implies a power law relation between both quantities

$$\bar{\sigma} = C\Big(\frac{\Delta E}{J}\Big)^{\alpha/\beta}, \tag{3.4}$$

with $C = \frac{A}{B^{\alpha/\beta}}$.

The linear fits of the curves in figures 3.11 and 3.12, which are presented in Table 3.3, show that in all cases $m = \frac{\alpha}{\beta} \approx 1$, which implies that the width of the entropy peaks is proportional to the energy gap of the corresponding avoided crossing

$$\bar{\sigma} = \frac{C}{J}\Delta E. \tag{3.5}$$

J	N_e	m	Δm	b	Δb
100	140	1.00398	0.00371	1.1408	0.06019
100	156	1.0109	0.005189	1.32628	0.08536
100	170	1.01285	0.006995	1.33982	0.1119
100	172	1.02573	0.01103	1.86144	0.202
100	174	1.06102	0.007393	2.2779	0.1632
100	186	1.01349	0.001369	2.39909	0.02395
100	196	1.00094	0.003417	3.35955	0.05828
200	340	1.04369	0.004264	2.31694	0.0912
500	850	1.01315	0.0237	1.67272	0.415

Table 3.3: Linear fits $y = mx + b$ to the curves in figures 3.11 and 3.12

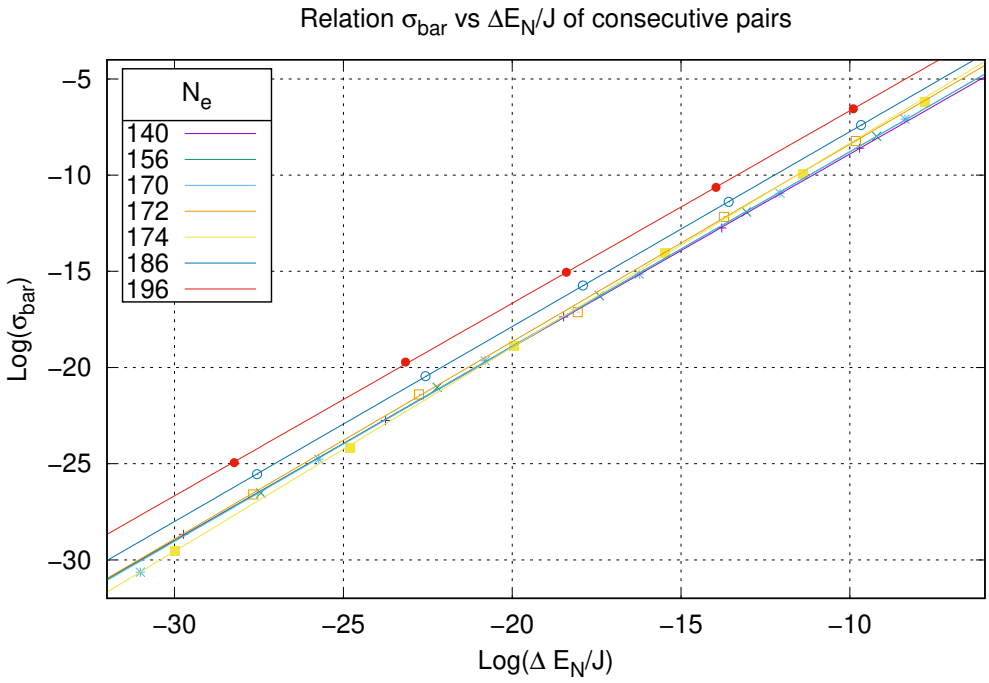

Figure 3.11: Logarithm of the width of the entropy peaks versus the logarithm of the energy gap in avoided crossings at different couplings γ_x^{AC} for $J = 100$. The slope of the curves $\frac{\alpha}{\beta} \approx 1.0$

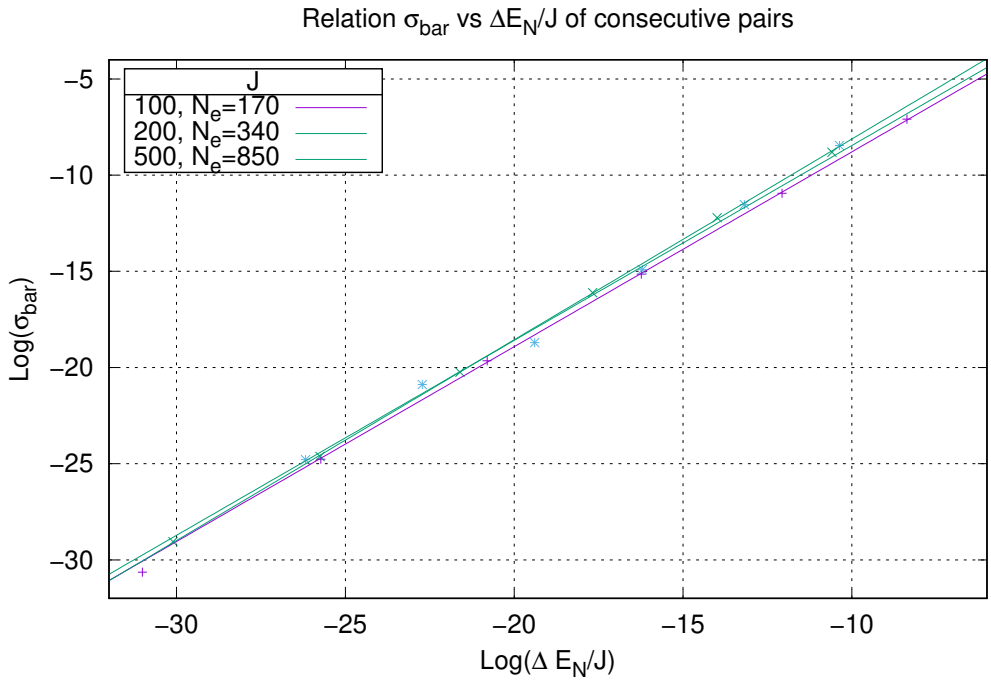

Figure 3.12: Logarithm of the width of the entropy peaks versus the logarithm of the energy gap in avoided crossings at similar values of the coupling parameter γ_x^{AC} and different system sizes. The slope of the curves is $\frac{\alpha}{\beta} \approx 1.0$

Conclusions

The LMG model shows avoided crossings at intermediate energy for certain values of the coupling parameter, γ_x^{AC}. The avoided crossing are accompanied by an increase and interchange of the Wehrl entropy of the levels involved in the avoided crossings, as the coupling parameter is varied around these values γ_x^{AC}. The increase of the Wehrl entropy is related, in turn, to a superposition of classical trajectories in the Husimi function of the energy levels participating in the avoided crossings.

In this thesis, the width of these Wehrl entropy peaks was determined for different avoided crossings and different system sizes. The width parameter of the Wehrl entropy curves decreases exponentially as we consider energy levels far above from the ESQPT critical energy, thus making difficult the detection of the superposition in the Husimi function for high energy crossings. As a consequence of this, since the dynamical tunneling and the superposition in the Husimi function are connected, dynamical tunneling at higher energies occurs in a very narrow interval of the coupling parameter.

The behaviour of the Wehrl entropy curves is similar along the energy spectrum, i.e. as we consider different avoided crossings or we vary the size of the system, it is possible to observe the increase and interchange of entropy between the levels participating in the avoided crossing, but the execution time and necessary precision to observe this behaviour increases to even 40 significant digits for high energy crossings.

It was found that the energy difference (gap) ΔE of the avoided crossings has a similar exponential decay as a function of the mean energy of the levels participating in the avoided crossings. Finally, it was also found that the width of the Wehrl entropy peaks is linearly related with the energy gap of the respective avoided crossing.This latter observation confirms that the presence of avoided crossings in the spectrum is associated to dynamical tunneling, but the tunneling occurs only in an exponentially small interval of the coupling parameter for avoided crossings taking place at large energies far above from the ESQPT critical energy.

A | LMG matrix representation

There are different ways to compute the matrix representation of the Hamiltonian. Numerically, one can define the action of $\hat{J}_\pm$ operators on the angular momentum basis and compute a particular element at each iteration. Here I chose to determine analytically equation (2.1) to define a function that returns the element (m', m) of the matrix representation at each iteration of the algorithm 1. First of all, let's adopt the next notation.

A.1 $C_\pm(J, m)$

This notation is introduced in order to simplify the expressions during analytical computation. Every book on quantum mechanics shows that the action of ladder operators $\hat{J}_\pm$ on the basis of eigenvectors of $\hat{J}^2$ and $\hat{J}_z$ operators is given by

$$J_+ |J,\, m\rangle = \hbar\sqrt{J(J+1) - m(m+1)}\, |J,\, m+1\rangle = \hbar C_+(J,m)\, |J,\, m+1\rangle \tag{A.1}$$

$$J_- |J,\, m\rangle = \hbar\sqrt{J(J+1) - m(m-1)}\, |J,\, m-1\rangle = \hbar C_-(J,m)\, |J,\, m-1\rangle \tag{A.2}$$

where

$$C_\pm(J,m) = \sqrt{J(J+1) - m(m\pm 1)} \tag{A.3}$$

Additionally, we also use the eigenvalues of $\hat{J}_z$ given by

$$\hat{J}_z |J,\, m\rangle = \hbar m\, |J,\, m\rangle \tag{A.4}$$

A.2 Analytical result

From LMG Hamiltonian in equation (1.5) we start by determining the action of each operator on the basis $|J,\, m\rangle$

$$\begin{aligned}
\hat{J}_x^2 \left|J,\, m\right\rangle &= \frac{1}{4}\left(\hat{J}_+^2 + \hat{J}_+\hat{J}_- + \hat{J}_-\hat{J}_+ + \hat{J}_-^2\right)\left|J,\, m\right\rangle \\
&= \frac{\hbar}{4}\Big[\hat{J}_+ C_+(J,m)\left|J,\, m+1\right\rangle + \hat{J}_+ C_-(J,m)\left|J,\, m-1\right\rangle + \\
&\quad + \hat{J}_- C_+(J,m)\left|J, m+1\right\rangle + \hat{J}_- C_-(J,m-1)\left|J,\, m-1\right\rangle\Big] \\
&= \frac{\hbar^2}{4}\Big[C_+(J,m)C_+(J,m+1)\left|J,m+2\right\rangle + C_-(J,m)C_+(J,m-1)\left|J,m\right\rangle + \\
&\quad + C_+(J,m)C_-(J,m+1)\left|J,m\right\rangle + C_-(J,m-1)C_-(J,m-1)\left|J,\, m-2\right\rangle\Big]
\end{aligned}$$

$$\begin{aligned}
\hat{J}_y^2 \left|J,\, m\right\rangle &= -\frac{1}{4}\left(\hat{J}_+^2 - \hat{J}_+\hat{J}_- - \hat{J}_-\hat{J}_+ + \hat{J}_-^2\right)\left|J,\, m\right\rangle \\
&= -\frac{\hbar}{4}\Big[\hat{J}_+ C_+(J,m)\left|J,\, m+1\right\rangle - \hat{J}_+ C_-(J,m)\left|J,\, m-1\right\rangle + \\
&\quad - \hat{J}_- C_+(J,m)\left|J, m+1\right\rangle + \hat{J}_- C_-(J,m-1)\left|J,\, m-1\right\rangle\Big] \\
&= -\frac{\hbar^2}{4}\Big[C_+(J,m)C_+(J,m+1)\left|J,m+2\right\rangle - C_-(J,m)C_+(J,m-1)\left|J,m\right\rangle + \\
&\quad - C_+(J,m)C_-(J,m+1)\left|J,m\right\rangle + C_-(J,m-1)C_-(J,m-1)\left|J,\, m-2\right\rangle\Big]
\end{aligned}$$

Since the $|J,m\rangle$ basis is orthonormal, the inner products or bra-kets will result in kronecker deltas.

$$\delta_{m',m} = \begin{cases} 1 & m' = m \\ 0 & m' \neq m \end{cases} \tag{A.5}$$

Now, it is possible to substitute these results to determine the desired expression.

$$\left\langle J,m'\right| \hat{H}_{LMG} \left|J,m\right\rangle = \epsilon_0 \left\langle J,\, m'\right| \left[\hat{J}_z + \left(\frac{\gamma_x}{2J-1}\right)\hat{J}_x^2 + \left(\frac{\gamma_y}{2J-1}\right)\hat{J}_y^2\right] \left|J\, m\right\rangle$$

$$
\begin{aligned}
&= \epsilon_0 \langle J,m| \left[\hat{J}_z |J,m\rangle + \left(\frac{\gamma_x}{2J-1}\right) \hat{J}_x^2 |J,\, m\rangle + \left(\frac{\gamma_y}{2J-1}\right) \hat{J}_y^2 |J,\, m\rangle \right] \\
&= \epsilon_0 \Bigg\{ \hbar m \delta_{m',m} + \\
&\quad + \left(\frac{\gamma_x}{2J-1}\right) \frac{\hbar^2}{4} \Big[C_+(J,m) C_+(J,m+1) \delta_{m',m+2} + C_-(J,m) C_+(J,m-1) \delta_{m',m} + \\
&\quad + C_+(J,m) C_-(J,m+1) \delta_{m',m} + C_-(J,m) C_-(J,m-1) \delta_{m',m-2} \Big] + \\
&\quad - \left(\frac{\gamma_y}{2J-1}\right) \frac{\hbar^2}{4} \Big[C_+(J,m) C_+(J,m+1) \delta_{m',m+2} - C_-(J,m) C_+(J,m-1) \delta_{m',m} + \\
&\quad - C_+(J,m) C_-(J,m+1) \delta_{m',m} + C_-(J,m) C_-(J,m-1) \delta_{m',m-2} \Big] \Bigg\}
\end{aligned}
$$

where the first row is due to green box, second and third row due to red box and the latter two rows are due to blue box. In general, this is the (m', m) matrix element of the Hamiltonian, and it depends on the size of the system J and the values of γ_x and γ_y. From here, i decided to go further and obtain a simplified expression where $\hbar = 1$, $\epsilon_0 = 1$ and $\gamma_y = 3\gamma_x$ given by

$$
\begin{aligned}
[\hat{H}_{LMG}]_{m',m} = m\delta_{m',m} + \left(\frac{\gamma_x}{4(2J-1)}\right) \Big\{ & - 2C_+(J,m) C_+(J,m+1) \delta_{m',m+2} + \\
& - 2C_-(J,m) C_-(J,m-1) \delta_{m',m-2} + 4 \Big[C_-(J,m) C_+(J,m-1) + \\
& + C_+(J,m) C_-(J,m+1) \Big] \delta_{m',m} \Big\}
\end{aligned} \tag{A.6}
$$

Note that

$$
\begin{aligned}
C_+(J,m-1) &= \sqrt{J(J+1) - (m-1)(m-1+1)} = C_-(J,m) \\
C_-(J,m+1) &= \sqrt{J(J+1) - (m+1)(m+1-1)} = C_+(J,m)
\end{aligned}
$$

and

$$
\begin{aligned}
C_-^2(J,m) + C_+^2(J,m)\delta_{m',m} &= J(J+1) - m(m-1) + J(J+1) - m(m+1) \\
&= 2J(J+1) - m(m-\cancel{1} + m + \cancel{1}) \\
&= 2[J(J+1) - m^2]
\end{aligned}
$$

then

$$[\hat{H}_{LMG}]_{m',m} = m\delta_{m',m} - \frac{\gamma_x}{2(2J-1)}\Big\{ C_+(J,m)C_+(J,m+1)\delta_{m',m+2} + \\ + C_-(J,m)C_-(J,m-1)\delta_{m',m-2} - 4\big[J(J+1)-m^2\big]\Big\} \tag{A.7}$$

This expression is equation (2.1) and allows to explore directly region III at EDoS.

A.3 Example

In order to validate the results in these sections, let's compute the case where $J = 1$. First, using the general expression(where $\gamma_x \neq \gamma_y$) with $\epsilon_0 = 1$, we know that $m = -1, 0, 1$.

$$[\hat{H}_{LMG}] = \begin{pmatrix} \langle 1,-1|\,\hat{H}\,|1,-1\rangle & \langle 1,-1|\,\hat{H}\,|1,0\rangle & \langle 1,-1|\,\hat{H}\,|1,1\rangle \\ \langle 1,0|\,\hat{H}\,|1,-1\rangle & \langle 1,0|\,\hat{H}\,|1,0\rangle & \langle 1,0|\,\hat{H}\,|1,1\rangle \\ \langle 1,1|\,\hat{H}\,|1,-1\rangle & \langle 1,1|\,\hat{H}\,|1,0\rangle & \langle 1,1|\,\hat{H}\,|1,1\rangle \end{pmatrix}$$

The non-zero contributions are given by

$$\begin{aligned} \langle 1,-1|\,\hat{H}\,|1,-1\rangle &= -\hbar + \frac{\gamma_x\hbar^2}{4}\big[C_-(1,-1)C_+(1,-2) + C_+(1,-1)C_-(1,0)\big] + \\ &\quad - \frac{\gamma_y\hbar^2}{4}\big[-C_-(1,-1)C_+(1,-2) - C_+(1,-1)C_-(1,0)\big] \\ &= -\hbar + \frac{\hbar^2}{4}\big[\gamma_x(0+2) - \gamma_y(0-2)\big] = -\hbar + \frac{\hbar^2}{2}(\gamma_x+\gamma_y) \\ \langle 1,-1|\,\hat{H}\,|1,1\rangle &= \frac{\hbar^2}{4}\big[\gamma_x C_-(1,1)C_-(1,0) - \gamma_y C_-(1,1)C_-(1,0)\big] = \frac{\hbar^2}{2}\big(\gamma_x-\gamma_y\big) \\ \langle 1,0|\,\hat{H}\,|1,0\rangle &= \cancel{(0)\hbar} + \frac{\gamma_x\hbar^2}{4}\big[C_-(1,0)C_+(1,-1) + C_+(1,0)C_-(1,1)\big] + \\ &\quad - \frac{\gamma_y\hbar^2}{4}\big[-C_-(1,0)C_+(1,-1) - C_+(1,0)C_-(1,1)\big] = \hbar^2\big(\gamma_x+\gamma_y\big) \end{aligned}$$

$$\begin{aligned} \langle 1,1|\,\hat{H}\,|1,-1\rangle &= \frac{\hbar^2}{4}\big[\gamma_x C_+(1,-1)C_+(1,0) - \gamma_y C_+(1,-1)C_+(1,0)\big] \\ &= \frac{\hbar^2}{2}(\gamma_x-\gamma_y) \end{aligned}$$

$$\begin{aligned}\langle 1,1|\,\hat{H}\,|1,1\rangle &= \hbar + \frac{\gamma_x\hbar^2}{4}\big[C_-(1,1)C_+(1,0) + C_+(1,1)C_-(1,2)\big] + \\ &- \frac{\gamma_y\hbar^2}{4}\big[-C_-(1,1)C_+(1,0) - C_+(1,1)C_-(1,2)\big] \\ &= \hbar + \frac{\hbar^2}{4}\big[\gamma_x(2+0) - \gamma_y(-2+0)\big] = \hbar + \frac{\hbar^2}{2}(\gamma_x+\gamma_y)\end{aligned}$$

and

$$\langle 1,-1|\,\hat{H}\,|1,0\rangle = \langle 1,0|\,\hat{H}\,|1,-1\rangle = \langle 1,0|\,\hat{H}\,|1,1\rangle = \langle 1,1|\,\hat{H}\,|1,0\rangle = 0$$

therefore

$$\begin{pmatrix} -\hbar + \frac{\hbar^2}{2}(\gamma_x+\gamma_y) & 0 & \frac{\hbar^2}{2}\big(\gamma_x-\gamma_y\big) \\ 0 & \hbar^2(\gamma_x+\gamma_y) & 0 \\ \frac{\hbar^2}{2}\big(\gamma_x-\gamma_y\big) & 0 & \hbar + \frac{\hbar^2}{2}\big(\gamma_x+\gamma_y\big) \end{pmatrix}$$

when $\hbar = 1$, $\gamma_y = 3\gamma_x$ and $\gamma_x = -1$

$$\begin{pmatrix} -1+2\gamma_x & 0 & -\gamma_x \\ 0 & 4\gamma_x & 0 \\ -\gamma_x & 0 & 1+2\gamma_x \end{pmatrix} = \begin{pmatrix} -3 & 0 & 1 \\ 0 & -4 & 0 \\ 1 & 0 & -1 \end{pmatrix}$$

This result is a reference for future comparison if need.

B | Catalog

Here, there are presented the results of computing Wehrl entropy around several avoided crossings (See tables 3.1 and).

B.1 $J = 100$

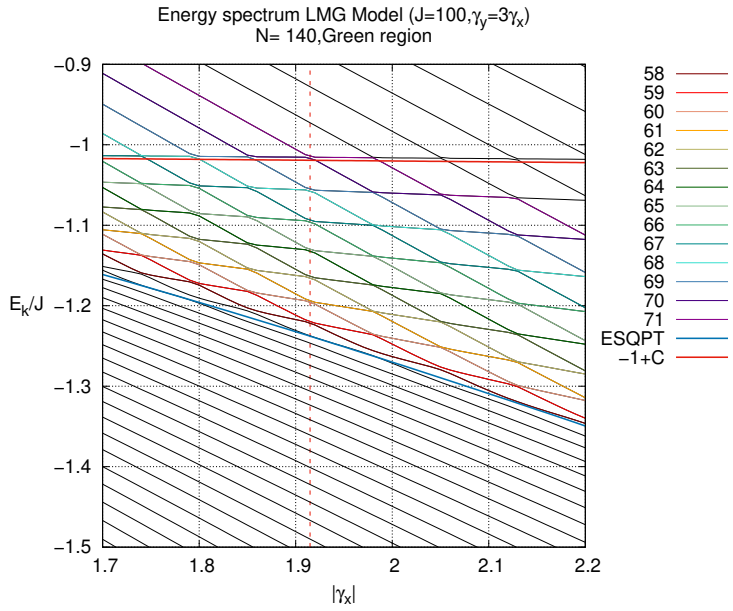

Figure B.1

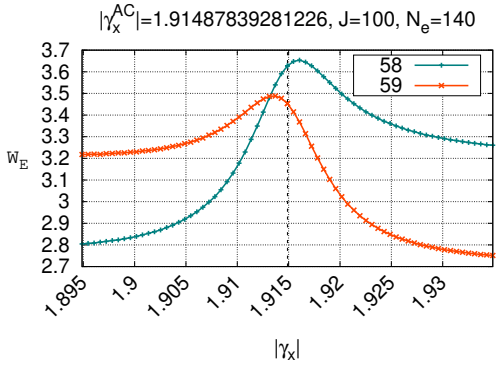

(a) 1st pair after ESQPT.

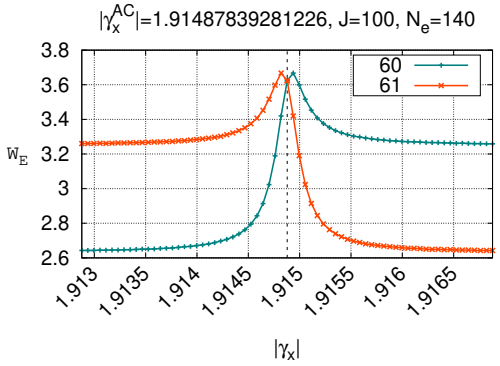

(b) 2nd pair after ESQPT.

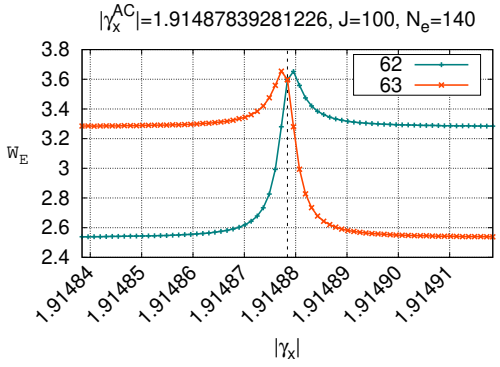

(c) 3rd pair

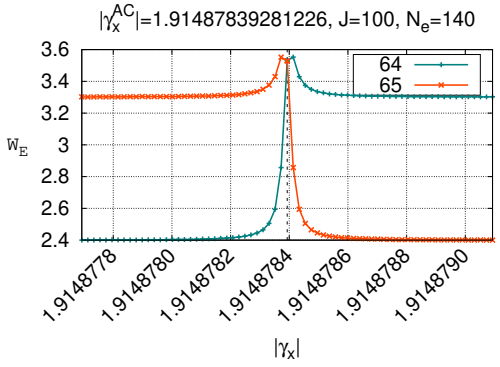

(d) 4th pair.

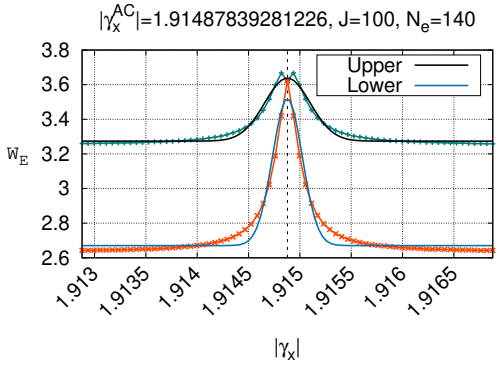

(e) Gaussian fit on 2nd pair data

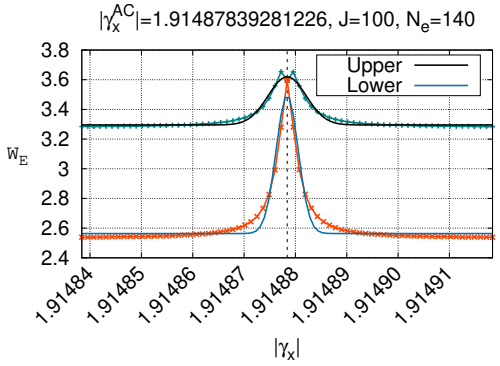

(f) Gaussian fit on 3rd pair data.

Figure B.2: Werhl entropy of four pairs of states after ESQPT for fixed values $J = 100$, $N_e = 140$ (a-d). Panels e and f show Gaussian fit examples.

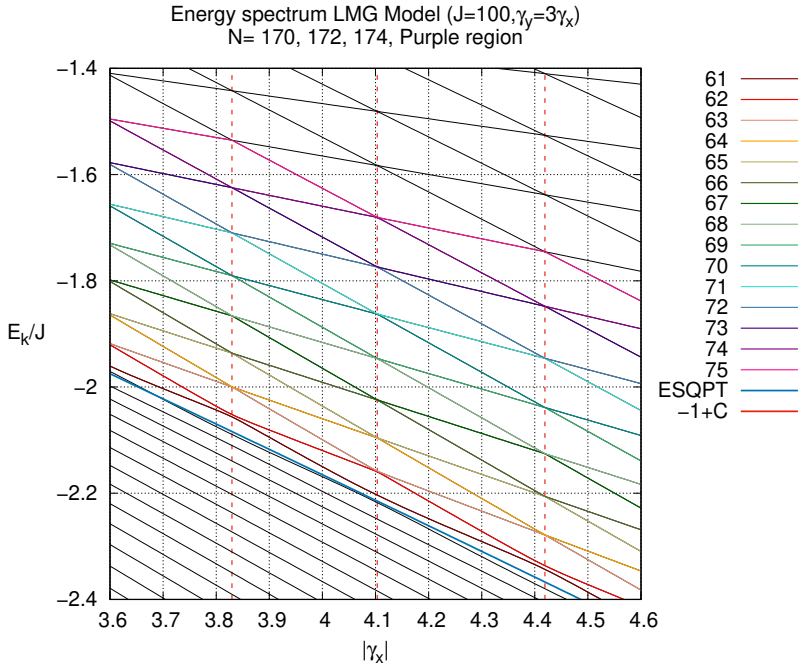

(a) 3 ACs.

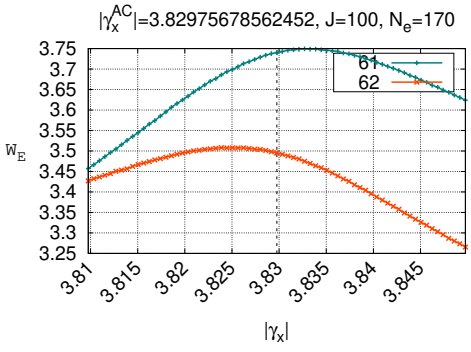

(b) Entropy gap at γ_x^{AC}

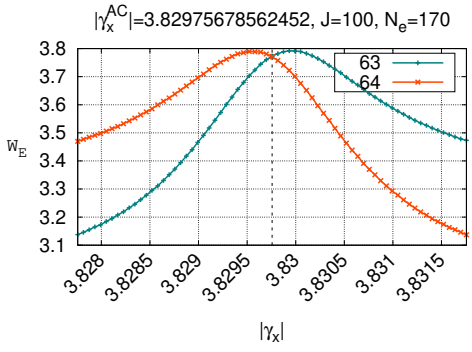

(c) Entropy crossing at γ_x^{AC}.

Figure B.3: Werhl entropy of the first two pairs of states after ESQPT for fixed values $J = 100$, $N_e = 170, 172, 174$.

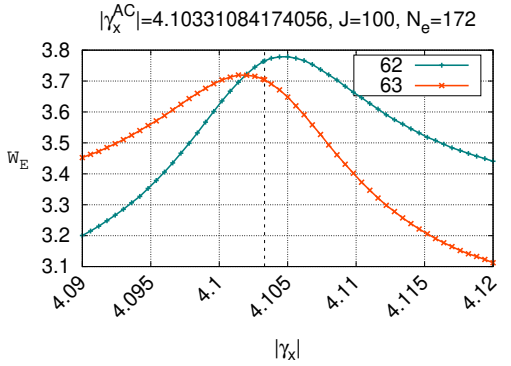

(a) 1st pair after ESQPT.

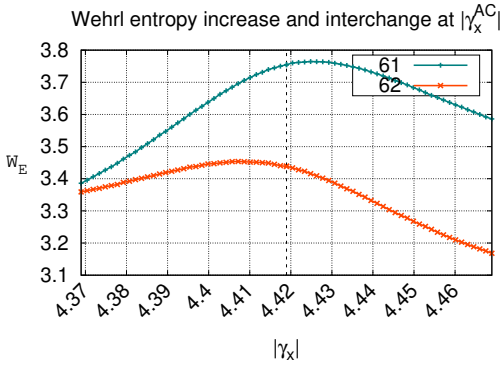

(b) 1st pair after ESQPT)

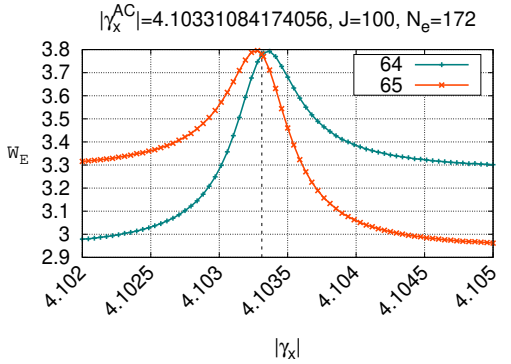

(c) 2nd pair after ESQPT.

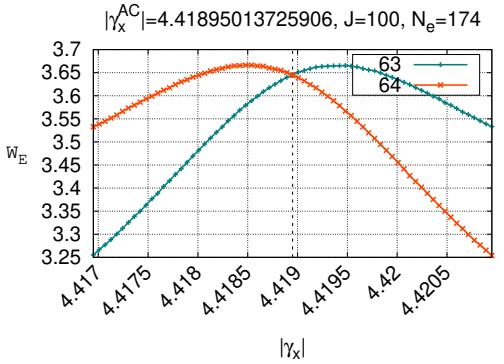

(d) 2nd pair after ESQPT

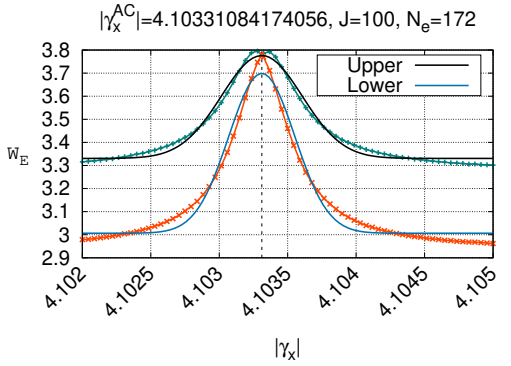

(e) Gaussian fit on 2nd pair data

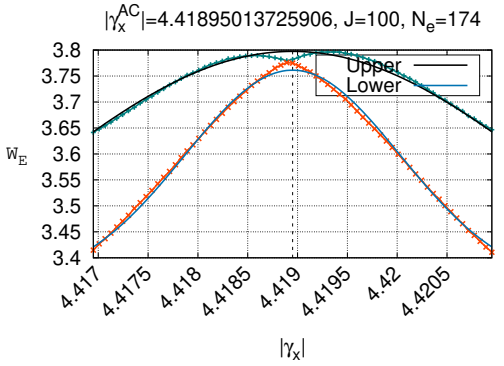

(f) Gaussian fit on 2nd pair data.

Figure B.4: Werhl entropy of first two pairs of states after ESQPT for fixed values $J = 100$, $N_e = 172$ (left column) $N_e = 174$ (right column).

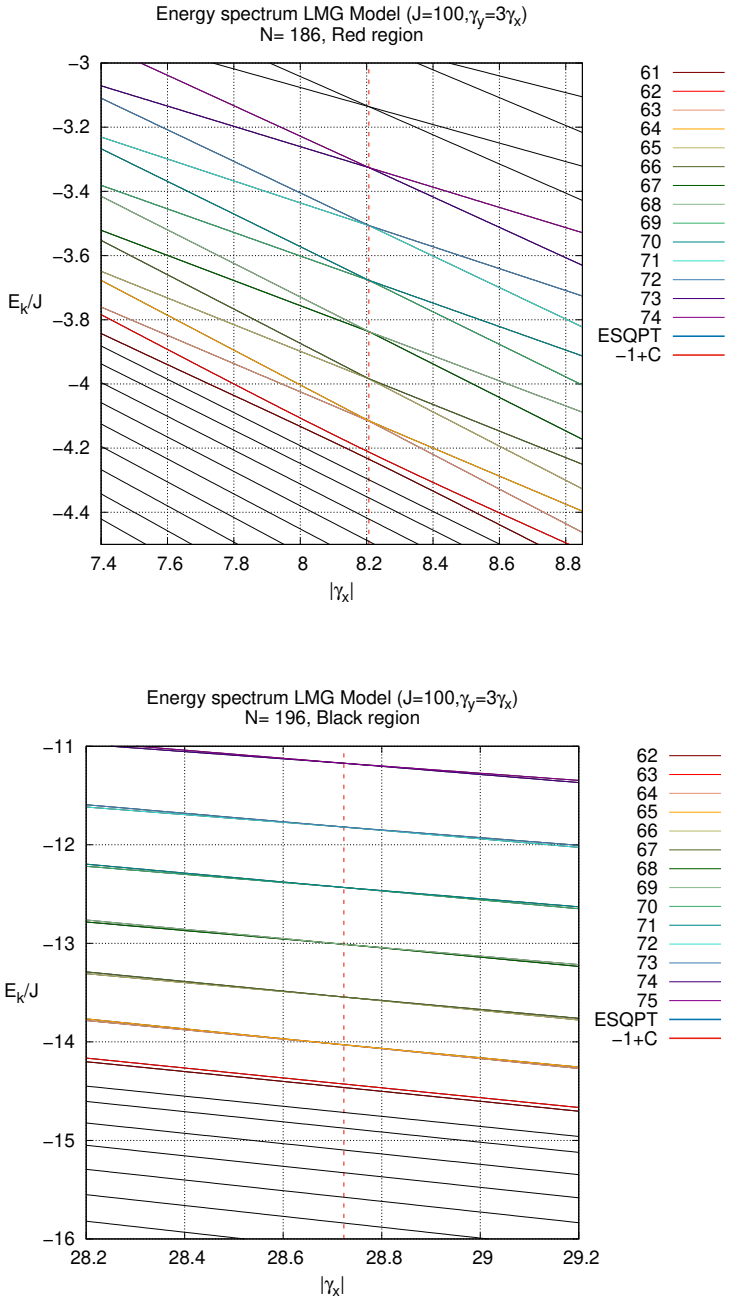

Figure B.5: Energy spectra for a fixed value of $J = 100$, $N_e = 186$ (top) and $N_e = 196$ (bottom).

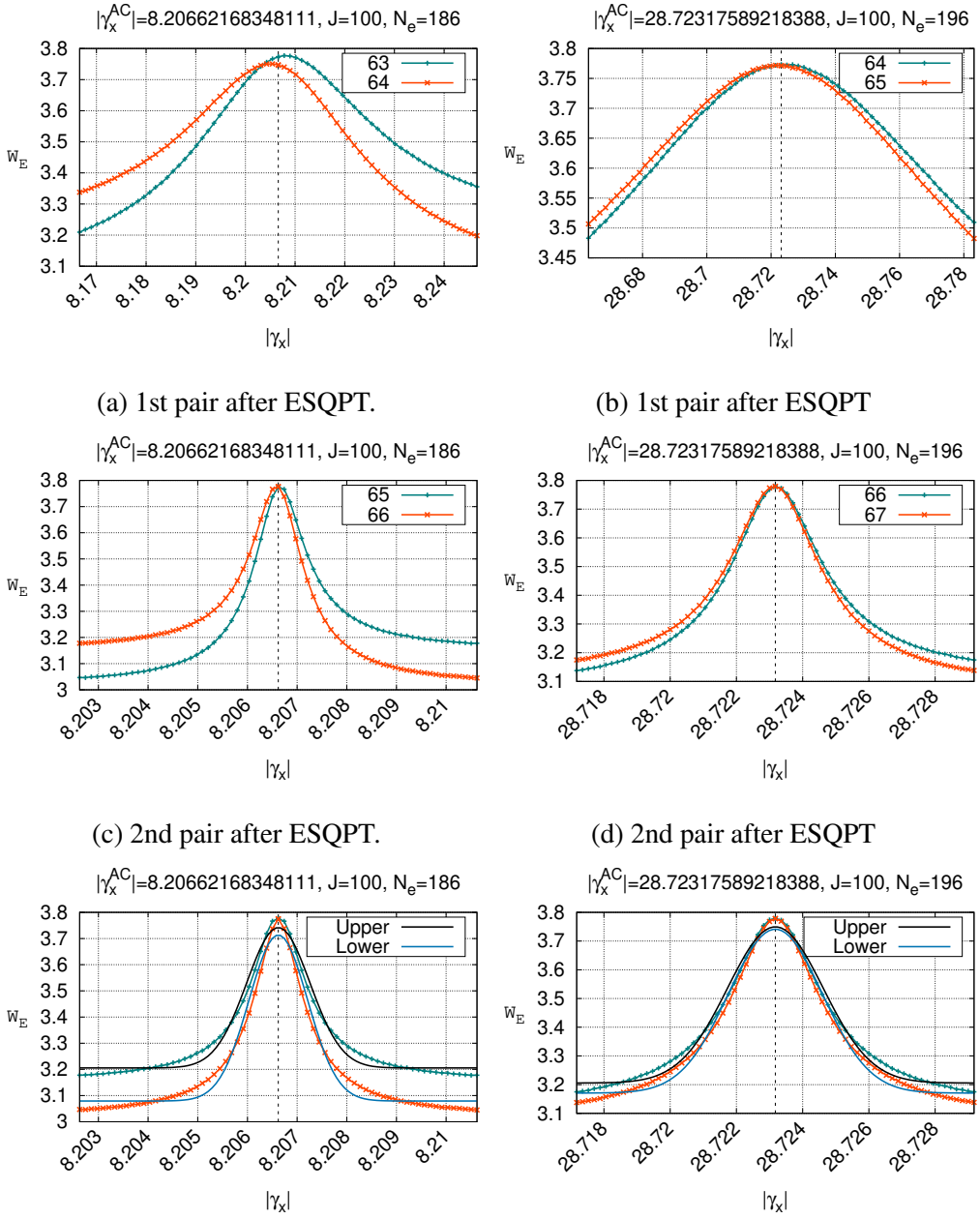

(a) 1st pair after ESQPT.

(b) 1st pair after ESQPT

(c) 2nd pair after ESQPT.

(d) 2nd pair after ESQPT

(e) Gaussian fit on 2nd pair data

(f) Gaussian fit on 2nd pair data.

Figure B.6: Werhl entropy of first two pairs of states after ESQPT for fixed values $J = 100$, $N_e = 186$ (left column) $N_e = 196$ (right column).

B.2 $J = 200$

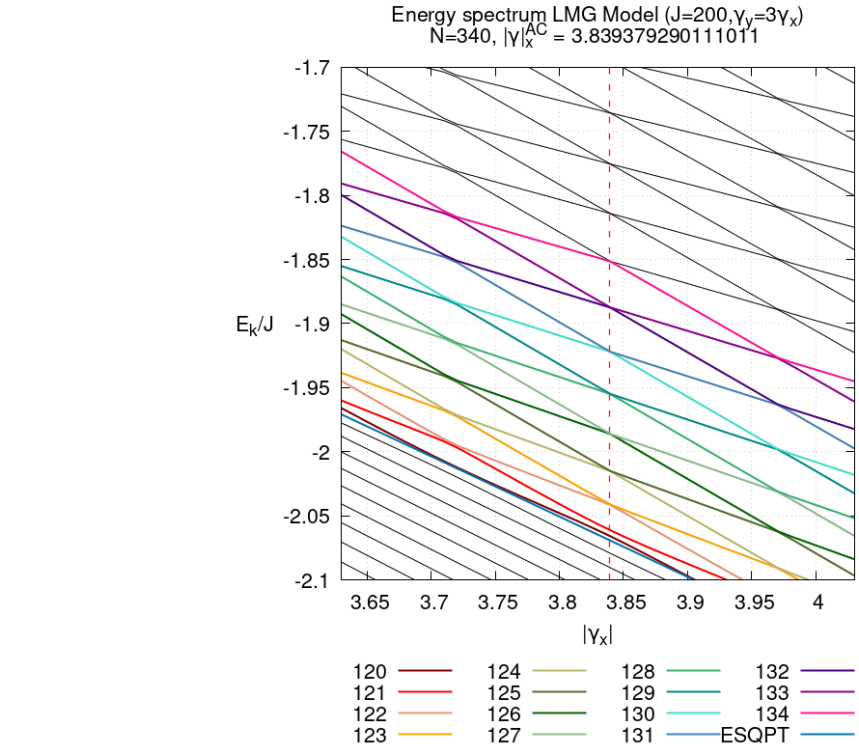

(a)

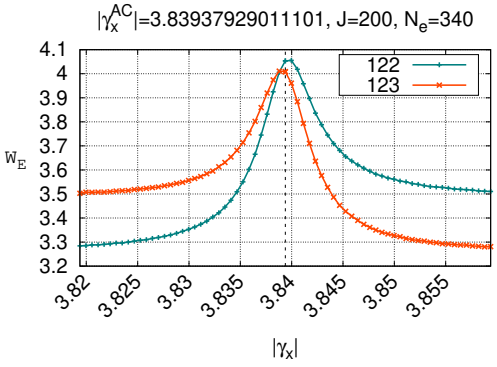

(b) Entropy gap at γ_x^{AC}

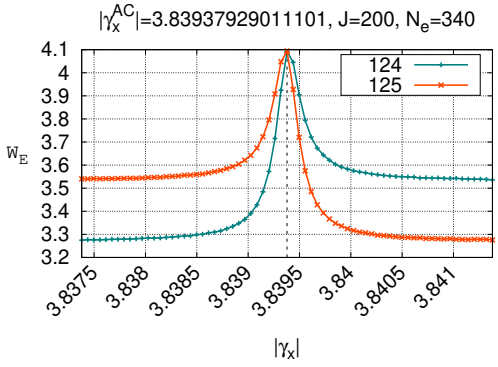

(c) Entropy crossing at γ_x^{AC}.

Figure B.7: Werhl entropy of the first two pairs of states after ESQPT for fixed values $J = 200$, $N_e = 340$.

Bibliography

[1] H. J. G., C. O., L.-P. R., and O. J. F., "Hartree-fock description of spin systems," Revista Mexicana de Física, vol. 53, pp. 41–47, 12 2007.

[2] C. O., L.-P. R. N.-A. E., and H. J. G., "Quantum phase transitions in the lmg model by means of quantum information concepts," Journal of Physics: Conference Series, vol. 387, p. 012021, 2012.

[3] L. F. Santos, M. Tá vora, and F. Pérez-Bernal, "Excited-state quantum phase transitions in many-body systems with infinite-range interaction: Localization, dynamics, and bifurcation," Physical Review A, vol. 94, 07 2016.

[4] I. Hobday, P. D. Stevenson, and J. Benstead, "Quantum computing calculations for nuclear structure and nuclear data," 2022.

[5] J. S. Ferreira and P. Ribeiro, "Lipkin-meshkov-glick model with markovian dissipation: A description of a collective spin on a metallic surface," Physical Review B, vol. 100, 11 2019.

[6] J. Ma and X. Wang, "Fisher information and spin squeezing in the lipkin-meshkov-glick model," 2009.

[7] E. Romera, O. Castaños, M. Calixto, and F. Pérez-Bernal, "Delocalization properties at isolated avoided crossings in lipkin–meshkov–glick type hamiltonian models," Journal of Statistical Mechanics: Theory and Experiment, vol. 2017, p. 013101, 01 2017.

[8] C. A. G. Rodríguez, "Correspondencia clásico-cuántica en el modelo de lipkin-meshkov-glick," 2015.

[9] D. J. Nader, C. A. González-Rodríguez, and S. Lerma-Hernández, "Avoided crossings and dynamical tunneling close to excited-state quantum phase transitions," Phys. Rev. E, vol. 104, p. 064116, Dec 2021.

[10] O. Castaños, R. López-Peña, J. G. Hirsch, and E. López-Moreno, "Classical and quantum phase transitions in the lipkin-meshkov-glick model," Phys. Rev. B, vol. 74, p. 104118, Sep 2006.

[11] P. Cejnar, P. Stránský, M. Macek, and M. Kloc, "Excited-state quantum phase transitions," Journal of Physics A: Mathematical and Theoretical, vol. 54, p. 133001, mar 2021.

[12] S. Keshavamurthy and P. Schlagheck, Dynamical Tunneling: Theory and Experiment. CRC Press, 1st ed., 2011.

[13] C. Cohen-Tannoudji, B. Diu, and F. Laloë, Quantum mechanics; 2nd ed. Germany: Wiley-VCH, 2020.

[14] M. J. Davis and E. J. Heller, "Quantum dynnamical tunneling in bound states," Chem. Phys., vol. 75(1), pp. 246–254, Jul 1981.

[15] S. Keshavamurthy, "Dynamical tunneling and control," 2011.

[16] H. J. Lipkin, N. Meshkov, and A. J. Glick, "Validity of many-body aproximation methods for a solvable model: (i). exact solutions and perturbation theory," Nuclear Physics, vol. 62, pp. 188–198, 02 1965.

[17] S. Lerma-H and J. Dukelsky, "The lipkin-meshkov-glick model from the perspective of the su(1,1) richardson-gaudin models," Journal of Physics: Conference Series, vol. 492, p. 012013, 03 2014.

[18] S. T. Thornton, Classical dynamics of particles and systems. Belmont, CA: Brooks/Cole, 5th ed. / stephen t. thornton, jerry b. marion. ed., 2004.

[19] M. Veronez and M. de Aguiar, "Phase space flow in the husimi representation," Journal of Physics A: Mathematical and Theoretical, vol. 46, 06 2013.

[20] D. Villaseñor, S. Pilatowsky-Cameo, M. A. Bastarrachea-Magnani, S. Lerma-Hernández, and J. G. Hirsch, "Quantum localization measures in phase space," Phys. Rev. E, vol. 103, p. 052214, May 2021.

[21] P. Stránský, M. Macek, and P. Cejnar, "Excited-state quantum phase transitions in systems with two degrees of freedom: Level density, level dynamics, thermal properties," Annals of Physics (New York), vol. 345, 6 2014.